NRL REPORT 3917

COPY NO. 152

DEVELOPMENT OF THE NRL ORCON TACTICAL MISSILE SIMULATOR

Charles F. White
Equipment Research Branch
Radio Division III

January 11, 1952

NAVAL RESEARCH LABORATORY

WASHINGTON, D.C.

CONTENTS

DISTRIBUTION

OpNav	
Attn: Code Op 342	1
Attn: Code Op 42	2
ONR	
Attn: Code 439	1
Attn: Code 451	1
Attn: Code 454	3
Attn: Code 459	3
Attn: Code 470	1
CO & Dir., USNEL	2
CDR, USNOTS	
Attn: Reports Unit	2
Supt., USNPGS	1
CDR, NATC, Patuxent River, Md.	
Attn: Electronics Test	1
CDR, NADC, Johnsville, Pa.	1
Wright Air Development Center	
Attn: Ch. Weapons Components Div., WCEOT	1
OCSigO	
Attn: Ch. Eng. & Tech. Div., SIGET	1
CO, SCEL	
Attn: SCEL Liaison Office	3
CO, Rome Air Development Center, Griffiss AFB, Rome, N. Y.	
Attn: ENR	1
CO, Air Force Cambridge Res. Center	
Attn: CRRS	1
Dir., NBS	
Attn: CRPL	1
RDB	
Attn: Information Requirements Branch	2
Attn; Navy Secretary	1
Dir., CADO	
Attn: BAU-CADO	1
Attn: CADO-E1	2
Naval Res. Sec., Science Div., Library of Congress	
Attn: Mr. J. H. Heald	2
ANAF/GM Mailing List No. 16, Part A	109

DEVELOPMENT OF THE NRL ORCON TACTICAL MISSILE SIMULATOR

INTRODUCTION

The concluding research under problem number R13-07 (ORCON) (Standing for ORganic CONtrol) by the Naval Research Laboratory will consist of studies under simulated tactical conditions. The background research and development details of the NRL ORCON Tactical Missile Simulator are presented in the present report together with a brief review of the over-all project.

As previously reported, the objective of project ORCON is the determination of whether or not a pigeon can be advantageously used in guided missile or pilotless aircraft steering.[1] The Navy Department requested review of the work of B. F. Skinner, et. al., at the University of Minnesota during World War II, in which preliminary tests were made to determine the feasibility of using pigeons to guide bombs to the target. The review disclosed that in restricted situations these birds are able to act as the sensing element in a simulated homing system with a surprising degree of success. Consequently, Naval Research Laboratory Problem No. R13-07 (ORCON) was set up and work is progressing in the investigation of the pigeon's ability to identify and to acquire a specified isolated target, its ability to retain a particular target, and its limitations in following a specified target (i.e., what are its target motion limitations).

In the preliminary investigations and studies of related training techniques, a machine previously referred to as the primary trainer has been used. The object tracked by the pigeon has taken a variety of forms from a moving strip, a moving spot of light projected on a frosted glass plate, to a projected image of a moving ship. Details of the results of tests of the pigeon's performance are reported elsewhere.[2] The present report is principally concerned with the research surrounding the development of a tactical missile simulator for studies in the final phases of the work under the project.

The Operational Research Branch, the Equipment Research Branch, and the Psychology Branch (each a subdivision of Radio Division III) have responsibilities under the ORCON project. The development of the missile simulator is an Equipment Research Branch responsibility.

---

[1] Taylor, F. V., Searle, L. V., and Stafford, B. H., "ORCON Part I—Outline of Proposed Research," NRL Ltr. Rpt. S-3600-157/50 (Secret), June 17, 1949.

[2] Stafford, B. H., Taylor, F. V., and Searle, L. V., "ORCON Part II—Report of Phase I Research and Band Pass Study," — Sec. V, NRL Ltr. Rpt. S-3600-157/50 (Secret), May 1, 1950

THE TACTICAL TRACKING PROBLEM

The tactical problem proposed for simulation is that of a pilotless aircraft or missile attacking a ship at sea moving along a straight line at constant speed. The simulator provides servo-loop closure in both elevation and train coordinates but ship motion is simulated only in the lateral plane. In fire control terminology, target motion in the slant plane, defined by the target line and the missile launching point, is simulated.

Characteristics of the flight path described above have been studied in connection with automatic radar homing devices and in training pilots of fighter or pursuit aircraft in aerial gunnery. The paths are known as pursuit curves and the differential equations of motion have been derived.[3]

Figure 1 shows the geometry from which the differential equations may be derived as follows:

Let a = speed of target,

b = speed of missile,

$k = \frac{a}{b}$,

x_o = initial rectangular component of distance between missile and target measured normally to the target path, and

y_o = initial rectangular component of distance between missile and target measured along the target path.

Then, at any time t after the beginning of the attack, the angle

$$m = 180^\circ - \alpha,$$

$$\tan m = -\tan \alpha,$$

$$\tan \alpha = \frac{at - y}{x}, \text{ and}$$

$$\frac{dy}{dx} = \tan m = -\tan \alpha = \frac{y - at}{x}. \tag{1}$$

Equation (1), when solved for t, becomes

$$t = \frac{y}{a} - \frac{x}{a}\frac{dy}{dx}. \tag{2}$$

If s is the distance along the curve travelled by the missile, then

$$s = bt, \quad \frac{s}{b} = \frac{y}{a} - \frac{x}{a}\frac{dy}{dx},$$

and

$$ks = y - x\frac{dy}{dx}. \tag{3}$$

[3] O.S.R.D. Report No. 3722 "Pursuit Curve Characteristics," February 1944

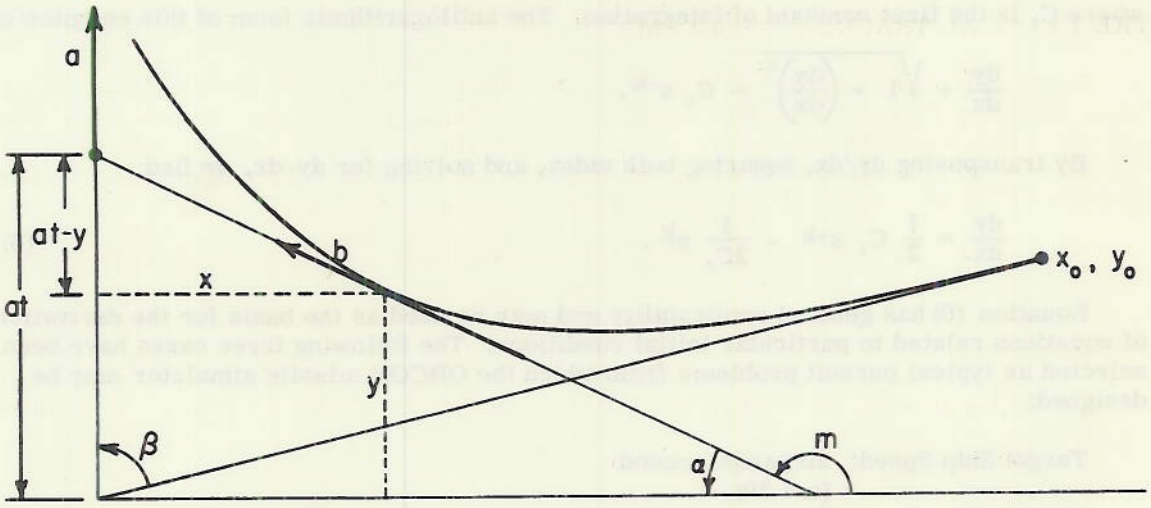

Figure 1 - Pursuit flight path geometry

Equation (3) is in a form suitable for differentiation. Differentiating with respect to x, we have

$$k\frac{ds}{dx} = \frac{dy}{dx} - \frac{dy}{dx} - x\frac{d^2y}{dx^2} = -x\frac{d^2y}{dx^2}.$$

But, from the differential triangle,

$$ds = \sqrt{(dx)^2 + (dy)^2},$$

and

$$\frac{ds}{dx} = \sqrt{1 + \left(\frac{dy}{dx}\right)^2}.$$

Hence,

$$k\sqrt{1 + \left(\frac{dy}{dx}\right)^2} = -x\frac{d^2y}{dx^2}. \tag{4}$$

In a form more suitable for integration, we therefore have the differential equation for the curve of pursuit as follows:

$$\frac{\frac{d}{dx}\left(\frac{dy}{dx}\right)}{\sqrt{1 + \left(\frac{dy}{dx}\right)^2}} = -\frac{k}{x}. \tag{5}$$

The left side of Equation (5) is of the form $dz/\sqrt{1 + z^2}$, so that the first integration yields

$$\ln\left(\frac{dy}{dx} + \sqrt{1 + \left(\frac{dy}{dx}\right)^2}\right) - \ln C_1 = -k \ln x,$$

where C_1 is the first constant of integration. The antilogarithmic form of this equation is

$$\frac{dy}{dx} + \sqrt{1 + \left(\frac{dy}{dx}\right)^2} = C_1 x^{-k}.$$

By transposing dy/dx, squaring both sides, and solving for dy/dx, we find

$$\frac{dy}{dx} = \frac{1}{2} C_1 x^{-k} - \frac{1}{2C_1} x^k. \tag{6}$$

Equation (6) has general applicability and may be used as the basis for the derivation of equations related to particular initial conditions. The following three cases have been selected as typical pursuit problems from which the ORCON missile simulator may be designed:

Target Ship Speed: 20 yards/second
(a = 20)
Missile Speed: 300 yards/second
(b = 300)

FLIGHT PATH 1

Launching Position: 9000 yards directly abeam
($x_0 = 9000$, $y_0 = 0$)

FLIGHT PATH 2

Launching Position: 9000 yards abeam of target course and 300 yards up-range
($x_0 = 9000$, $y_0 = 300$)

FLIGHT PATH 3

Launching Position: 9000 yards abeam of target course and 600 yards up-range
($x_0 = 9000$, $y_0 = 600$)

Continuing with the derivation of the equations for the pursuit curves, for Flight Path 1 initial conditions the constant of integration in Equation (6) is determined as follows:

$$\frac{dy}{dx} = 0 \quad \text{when } y = 0, x = x_0 = 9000.$$

Hence,

$$\frac{C_1}{2} x_0^{-k} - \frac{1}{2C_1} x_0^k = 0, \text{ or } C_1 = \pm x_0^k.$$

The proper sign for C_1 is evidently minus, since this will ensure that, for $x/x_0 < 1$, dy/dx is always minus, as it should be according to Figure 1. Hence,

$$\frac{dy}{dx} = \frac{1}{2}\left(x_0^{-k} x^k - x_0^k x^{-k}\right). \tag{7}$$

Substituting the value $x_0 = 9000$ and $k = 1/15$,

FOR FLIGHT PATH 1

$$\frac{dy}{dx} = 0.27249\, x^{\frac{1}{15}} - \frac{0.91746}{x^{\frac{1}{15}}}. \tag{8}$$

A second integration yields

$$y = 0.25546\, x^{\frac{16}{15}} - 0.98300\, x^{\frac{14}{15}} + 602.6786. \tag{9}$$

For this case, Equation (2) becomes

$$t = \frac{y}{20} - \frac{x}{20}\frac{dy}{dx}. \tag{10}$$

Equations (8), (9), and (10) may now be used to determine values at any particular point of interest. For the purposes of the ORCON simulator design, a lethal range of 600 yards may be assumed in view of the target and missile speeds. The values of Table 1 result.

TABLE 1
Flight Path 1 Computed Values

LAUNCHING POSITION: X_0 = 9000 YDS, y_0 = 0
TARGET SHIP SPEED: 20 YD/SEC
MISSILE SPEED: 300 YD/SEC

x (yd)	$\frac{dy}{dx}$	α (°)	y (yd)	t (sec)
600	-0.18152	10.29	452.44	28.068
620	-0.17930	10.17	448.83	28.000
640	-0.17715	10.05	445.27	27.932

Repeating the process,

FOR FLIGHT PATH 2

$$\frac{dy}{dx} = 0.28173\, x^{\frac{1}{15}} - \frac{0.88738}{x^{\frac{1}{15}}}, \tag{11}$$

$$y = 0.26412\, x^{\frac{16}{15}} - 0.95076\, x^{\frac{14}{15}} + 601.61, \tag{12}$$

and, as before,

$$t = \frac{y}{20} - \frac{x}{20}\frac{dy}{dx}. \tag{10}$$

The values of Table 2 result.

[redacted]

TABLE 2
Flight Path 2 Computed Values

LAUNCHING POSITION: $X_0 = 9000$ YDS, $y_0 = 300$ YDS
TARGET SHIP SPEED: 20 YD/SEC
MISSILE SPEED: 300 YD/SEC

x (yd)	$\frac{dy}{dx}$	α (°)	y (yd)	t (sec)
600	-0.14773	8.40	471.96	28.030
608	-0.14644	8.33	470.78	27.991
620	-0.14552	8.26	469.03	27.962

Again, repeating the process,

FOR FLIGHT PATH 3

$$\frac{dy}{dx} = 0.29126\, x^{\frac{1}{15}} - \frac{0.858324}{x^{\frac{1}{15}}}, \tag{13}$$

$$y = 0.27306\, x^{\frac{16}{15}} - 0.91963\, x^{\frac{14}{15}} + 601.29, \tag{14}$$

and, as before,

$$t = \frac{y}{20} - \frac{x}{20}\frac{dy}{dx}. \tag{10}$$

The values of Table 3 result.

TABLE 3
Flight Path 3 Computed Values

LAUNCHING POSITION: $X_0 = 9000$ YDS, $y_0 = 600$ YDS
TARGET SHIP SPEED: 20 YD/SEC
MISSILE SPEED: 300 YD/SEC

x (yd)	$\frac{dy}{dx}$	α (°)	y (yd)	t (sec)
600	-0.11416	6.51	492.05	28.027
608	-0.11327	6.46	491.14	28.000
638	-0.11005	6.28	487.44	27.883

Using second differences, the values presented in Tables 1, 2, and 3 may be used to determine the rate of change of missile heading angle with the following results as found for the 28 second point:

FLIGHT PATH	RATE OF CHANGE OF HEADING
1	1.850 degrees/second
2	1.765
3	1.571
AVERAGE	1.709 degrees/second

Note that the rate of change of heading for Flight Path 2, as evaluated after 28 seconds of flight, is close to the average of the three cases as is expected from the intermediate launching position. It was decided to design a projector position-control cam for the ORCON simulator on the basis of Flight Path 2 curve of pursuit. Graphical means were employed in drawing the flight paths given in Figure 2.

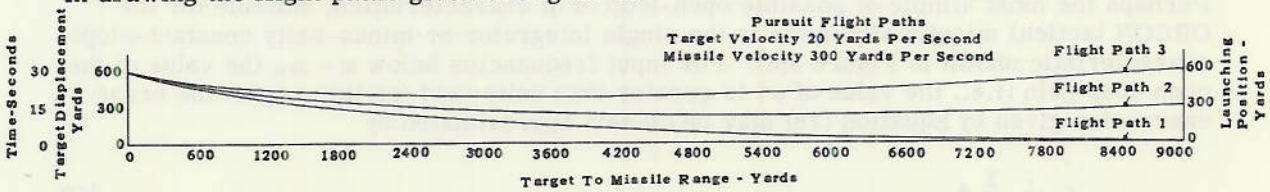

Figure 2 - Missile pursuit flight paths against a straight-line target course for design of a tactical problem simulator

Denoting missile heading angle by the symbol ϕ, the time rate of change of heading angle or angular velocity by $\dot{\phi}$, and the time rate of change of angular velocity or angular acceleration by $\ddot{\phi}$, we have the basic characteristics of the input signal to be imposed upon the tactical missile simulator servo system as presented in Figure 3.

SELECTION OF SERVO SYSTEM FREQUENCY RESPONSE CHARACTERISTICS

An approximation to the tracking error to be expected with a servo system may be derived as follows. Consider the generalized representation of a servo system shown in Figure 4, in which

ϕ_i = input (equivalent angle),

ϕ_o = output (equivalent angle),

μ = forward gain characteristic, and

β = feedback characteristic.

From the equation

$$\phi_o = \phi_i \mu + \mu\beta\phi_o, \qquad (15)$$

the output is found equal to

$$\phi_o = \frac{\mu}{1 - \mu\beta}\,\phi_i. \qquad (16)$$

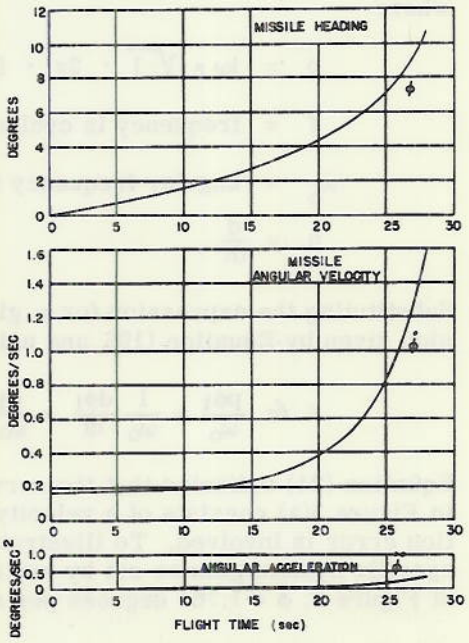

Figure 3 - Typical pursuit curve characteristics

In the servo systems under consideration, $\beta = -1$ and the output becomes

$$\phi_o = \frac{\mu}{1+\mu}\,\phi_i \,. \tag{17}$$

The input-output error expression, ϵ, may be written as:

$$\begin{aligned} \epsilon &= \phi_i - \phi_o, \\ &= \left(1 - \frac{\mu}{1+\mu}\right)\phi_i, \\ &= \left(\frac{1}{1+\mu}\right)\phi_i. \end{aligned} \tag{18}$$

Perhaps the most simple of possible open-loop or μ characteristics, suitable for the ORCON tactical missile simulator is the single integrator or minus-unity constant-slope characteristic shown in Figure 5(a). For input frequencies below $\omega = \omega_o$, the value of the open-loop gain (i.e., the value of μ) is greater than unity; and for this region the error expression given by Equation (18) may be closely approximated by

$$\epsilon \doteq \frac{1}{\mu}\,\phi_i \,. \tag{19}$$

The characteristic of Figure 5(a) may be expressed mathematically by

$$\mu \doteq \frac{\omega_o}{p}, \tag{20}$$

where

$p \equiv j\omega = \sqrt{-1} \cdot 2\pi \cdot f,$

f = frequency in cycles per second,

ω_o = angular frequency for unity gain, and

$p \equiv \frac{d}{dt}$.

Substituting the expression for μ given by Equation (20) into the approximate error expression given by Equation (19), and using the transient analysis definition of p (i.e., $p \equiv d/dt$),

$$\epsilon \doteq \frac{p\phi_i}{\omega_o} = \frac{1}{\omega_o}\frac{d\phi_i}{dt} = \frac{\dot{\phi}_i}{\omega_o} \,. \tag{21}$$

Equation (21) indicates that the servo-system tracking error for the characteristic shown in Figure 5(a) consists of a velocity error only; no component position error or acceleration error is involved. To illustrate the significance of the error expression, consider a specific system gain as set by making $\omega_o = 2$ radians per second. For the 28-second point of Figure 3, $\dot{\phi} = 1.765$ degrees per second. Thus,

$$\epsilon = \frac{1.765}{2} = 0.883 \text{ degree} \,. \tag{22}$$

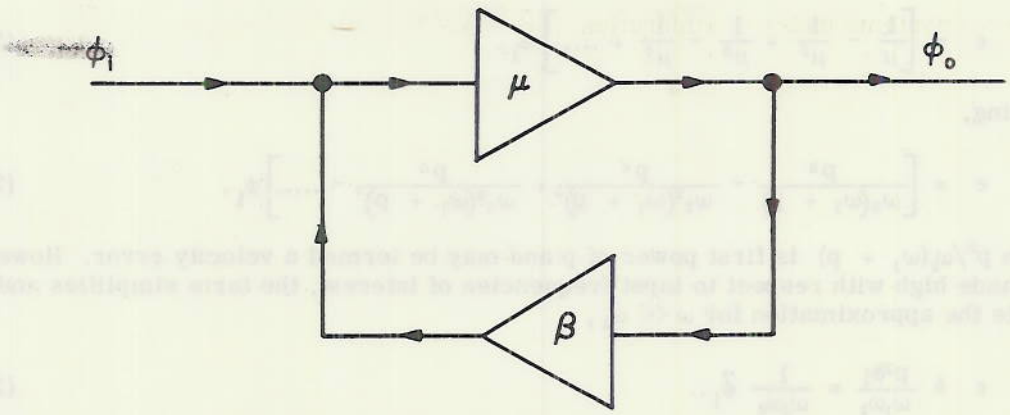

Figure 4 - Generalized representation of a servo system

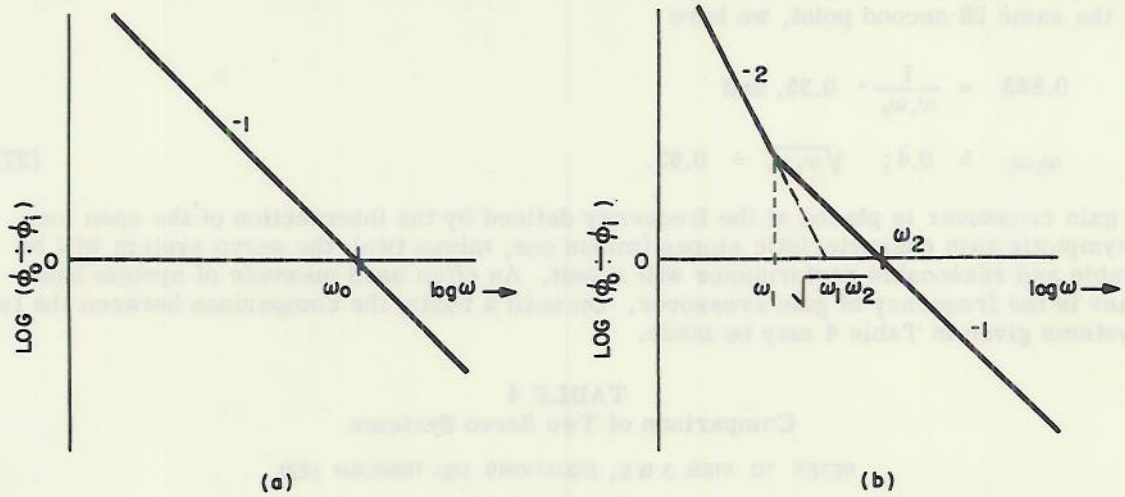

Figure 5 - Servo-system open-loop asymptotic gain characteristics for consideration

Another possible open-loop or μ characteristic is that shown in Figure 5(b). This characteristic would be used in an actual missile servo-system and is not suggested for the simulator. The expression for open-loop gain is

$$\mu = \frac{\omega_2}{p}\left(\frac{\omega_1}{p}\right)\left(\frac{\omega_1 + p}{\omega_1}\right),$$

$$\mu = \frac{\omega_2 (\omega_1 + p)}{p^2} . \tag{23}$$

Before substituting the value of μ given by Equation (23), make a series expansion of the expression for error given by Equation (18). This gives

$$\epsilon = \left(\frac{1}{1 + \mu}\right)\phi_i , \tag{18}$$

$$\epsilon = \left[\frac{1}{\mu} - \frac{1}{\mu^2} + \frac{1}{\mu^3} - \frac{1}{\mu^4} + \cdots\right]\phi_i . \tag{24}$$

Substituting,

$$\epsilon = \left[\frac{p^2}{\omega_2(\omega_1 + p)} - \frac{p^4}{\omega_2^2(\omega_1 + p)^2} + \frac{p^6}{\omega_2^3(\omega_1 + p)^3} - \cdots\right]\phi_i . \tag{25}$$

The term $p^2/\omega_2(\omega_1 + p)$ is first power of p and may be termed a velocity error. However, if ω_1 is made high with respect to input frequencies of interest, the term simplifies and we may write the approximation for $\omega \ll \omega_1$,

$$\epsilon \doteq \frac{p^2\phi_i}{\omega_1\omega_2} = \frac{1}{\omega_1\omega_2}\ddot{\phi}_i . \tag{26}$$

Thus, for servo system designs where ω_1 is much greater than the expected input frequencies, the total error is closely approximated by only an acceleration term. If the same error is allowed as computed in Equation (22) and the acceleration is read from Figure 3 at the same 28 second point, we have

$$0.883 = \frac{1}{\omega_1\omega_2} \cdot 0.35, \text{ and}$$

$$\omega_1\omega_2 \doteq 0.4; \quad \sqrt{\omega_1\omega_2} \doteq 0.63. \tag{27}$$

If gain crossover is placed at the frequency defined by the intersection of the open loop asymptotic gain characteristic slopes (minus one, minus two), the servo system will be stable and reasonable performance will result. An often used measure of system bandpass is the frequency of gain crossover. On such a basis, the comparison between the two systems given in Table 4 may be made.

TABLE 4
Comparison of Two Servo Systems

REFER TO FIGS. 3 & 5, EQUATIONS (18) THROUGH (22)

OPEN LOOP GAIN	−1 SLOPE	−2, −1 SLOPES
FIGURE	5 (a)	5 (b)
ERROR, ϵ	FOR $\omega \ll \omega_o$ $\frac{\dot{\phi}_i}{\omega_o}$	FOR $\omega \ll \omega_1$ $\frac{\ddot{\phi}_i}{\omega_1\ \omega_2}$
28 SECOND POINT (FIG. 3)	$\dot{\phi}_i = 1.765$	$\ddot{\phi}_i = 0.35$
$\epsilon = 0.883$	$\omega_o = 2$	$\omega_1 = 0.63$

The major result of using the characteristic shown in Figure 5(b) instead of the single-integrator characteristic shown in Figure 5(a) is seen from Table 4 to be an almost two-octave reduction in system bandpass requirements for a given tracking error. A reduction

in bandpass means less system noise and an easing of system component specifications. These factors offset the attendant reduction in gain and phase margin over that obtained with the single-integrator characteristic.

For the tactical missile situation, the servo system is mounted in an airframe that has forward motion through the air while in use. For a constant velocity missile, it may be stated that the rate of change of heading is proportional to a control-surface position and the time in that position. More exactly, we may write

$$\dot{\phi} = f(\delta, t),$$
$$\phi = \int \delta \, dt, \tag{28}$$

where

ϕ = missile heading,

δ = control surface angle (a function of time),

dt = differential time, and

$\int$ = integral.

The foregoing is meant to show the fundamental relationship, in the tactical application, between pursuit homing dynamics and a servo system having a single integrator or minus-one slope open-loop gain characteristic designed for heading control of a forward moving airframe. It is seen that the servo system as employed for control of a mirror position in a laboratory bench set-up must have a basic single integrator characteristic. The more complex characteristic of Figure 5(b) may be used, however, without violation of the basic requirement. By using the characteristic of Figure 5(a) for the ORCON tactical-missile simulator certain advantages of ease of system balance and interpretation of results are retained. In the laboratory, system noise is less than in an actual tactical-missile system and bandpass reduction is relatively less important.

As previously reported,[4] there is evidence which suggests that the pigeon is an approximately linear operator for target velocities below a certain value, and that input motion having frequencies up to a certain value are followed with reasonable fidelity. The experimental limits reported were five inches per second image velocities and seven radians per second image frequencies, respectively. It was considered that these values could, with reasonable assurance, be used in designing servo equipment for a pigeon in a similar tracking situation.

The values used in the illustration of the significance of the error characteristics of the two systems are well within the pigeon's ability. As will be seen later, the magnitude of the error is also well within practical specifications. Accordingly, the task to be simulated should prove to be well within the tracking ability of the pigeon.

TACTICAL MISSILE SIMULATOR SERVO SYSTEM

From the outset, the development of the NRL ORCON tactical missile simulator was influenced by the necessity of training the operating subjects as well as of making final

4 Stafford, Bruce H., op. cit.

tests of their performance under conditions simulating a tactical situation. Figure 6 shows the simulator components from a servo-system block diagram point of view.

The operating subject is placed in a position near the position-voltage converter plate such that the plate may be probed. The projected light-patterns that are reflected by the mirror form images on the ground glass surface of the converter plate. The angular deflection of the projector (labeled θ_{in} on Figure 6) appear as image position deflections, D_{in}. When the probe (directly connected to ground) is touched against the converter plate, a voltage field pattern appears with resulting voltage pulse outputs whose magnitude is related to the position of the contact point. The left-right or train axis, voltage E_1, is illustrated in Figure 6. An identical up-down or elevation axis is provided in the system but is not shown in the simplified block diagram.

The voltage pulse is amplified and stretched to increase the signal-to-noise ratio. Other gating signals and signals to the scoring system developed within the pulse amplifier-stretcher unit are described in detail in a later section. The varying dc pulse stretcher output signal, E_2, is modified by the tracking equalizer network to the voltage labeled E_3.

The block diagram of Figure 6 shows the three voltages E_3, E_{SG}, and E_M in series to form the total voltage E_4. The voltage E_{SG} is introduced by a signal generator. A zero-reference adjustment is provided so that a particular position of a cam-controlled potentiometer type of signal generator may be selected as a reference point. This signal generator is used only for open-loop training of the subject. In a similar circuit arrangement, the voltage E_M appears as a mirror position feedback signal since direct mechanical connection exists between the mirror position feedback potentiometer and the mirror itself. A mirror position reference potentiometer is provided to permit easy manual readjustment of the zero or reference position of the mirror. It should be noted that E_4 equals E_3 when the mirror servo motor field excitation is disconnected and no excitation is applied to the signal generator potentiometer as is the case during balancing adjustments.

The voltage E_8 acts to modulate a 60-cycle carrier voltage which is amplified by the ac servo amplifier to produce the voltage E_5. The servo motor is driven in a direction and at a rate dependent upon the polarity and the magnitude, respectively, of the voltage E_5. The servo motor shaft is directly coupled to a tachometer generator which develops a feedback signal proportional to the rate of change of mirror position. This signal, voltage E_6, is modified by the feedback network to E_7. The modulator input signal, E_8, is the sum of E_4 and E_7. The primary function of the servo motor is to control the position of the mirror itself. This is accomplished through a gear reduction as shown in Figure 6. The servo system follows up the input signal introduced at the projector by compensatory changes of the mirror angle. Of course, the operation is dependent upon a reasonably continuous flow of position-to-voltage information at the transducer plate. The limits of "reasonable" are discussed in later portions of the report.

Figure 7 shows a functional diagram of the simulator servo system in which the correspondence with the equivalent portions of the block diagram of Figure 6 is evident. The equations and the magnitudes of the transfer gain constants given in Figure 7 represent the end result of detail analyses and measurements made upon the functioning equipment. The information is presented here so that an early over-all view of the completed system may be obtained. In particular, note that the interrelationship of the projector-mirror-plate mechanism has been shown in a functional manner leading to a clear understanding of their separate as well as their combined performance. Conversion gains are indicated by K with identifying subscripts. Where the conversion gains are a complex function of frequency, the notation G(p) is employed. The symbol ω with a subscript means a particular value of frequency in radians per second. The symbol p is the complex frequency variable defined by $p \equiv j\omega = \sqrt{-1} \cdot 2\pi \cdot f$, where f is frequency in cycles per second. A second definition of p, the transient analysis equivalence of $p \equiv d/dt$, is used in converting to the time rate of change of the variable indicated by θ.

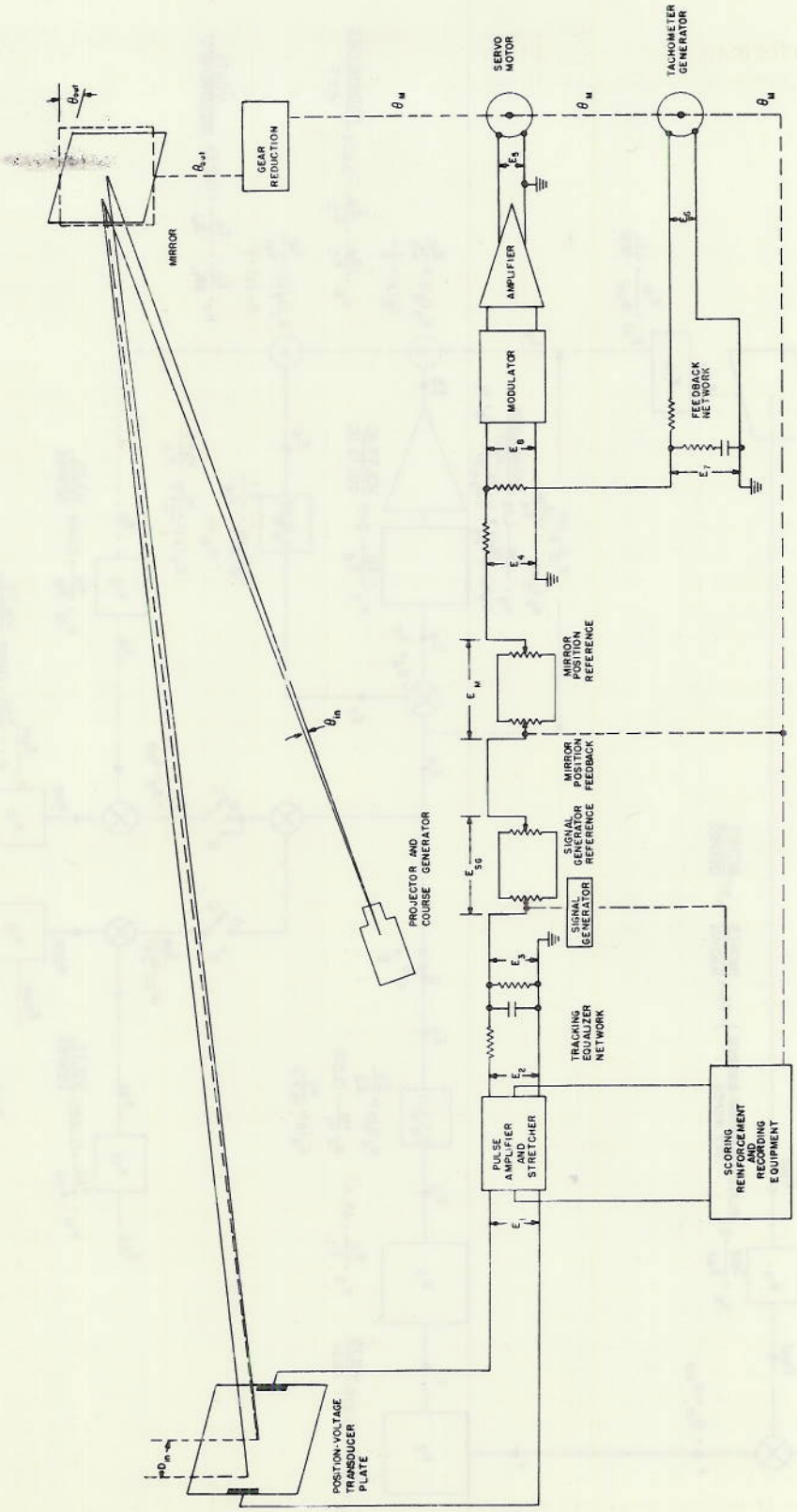

Figure 6 - Simulator servo-system block diagram

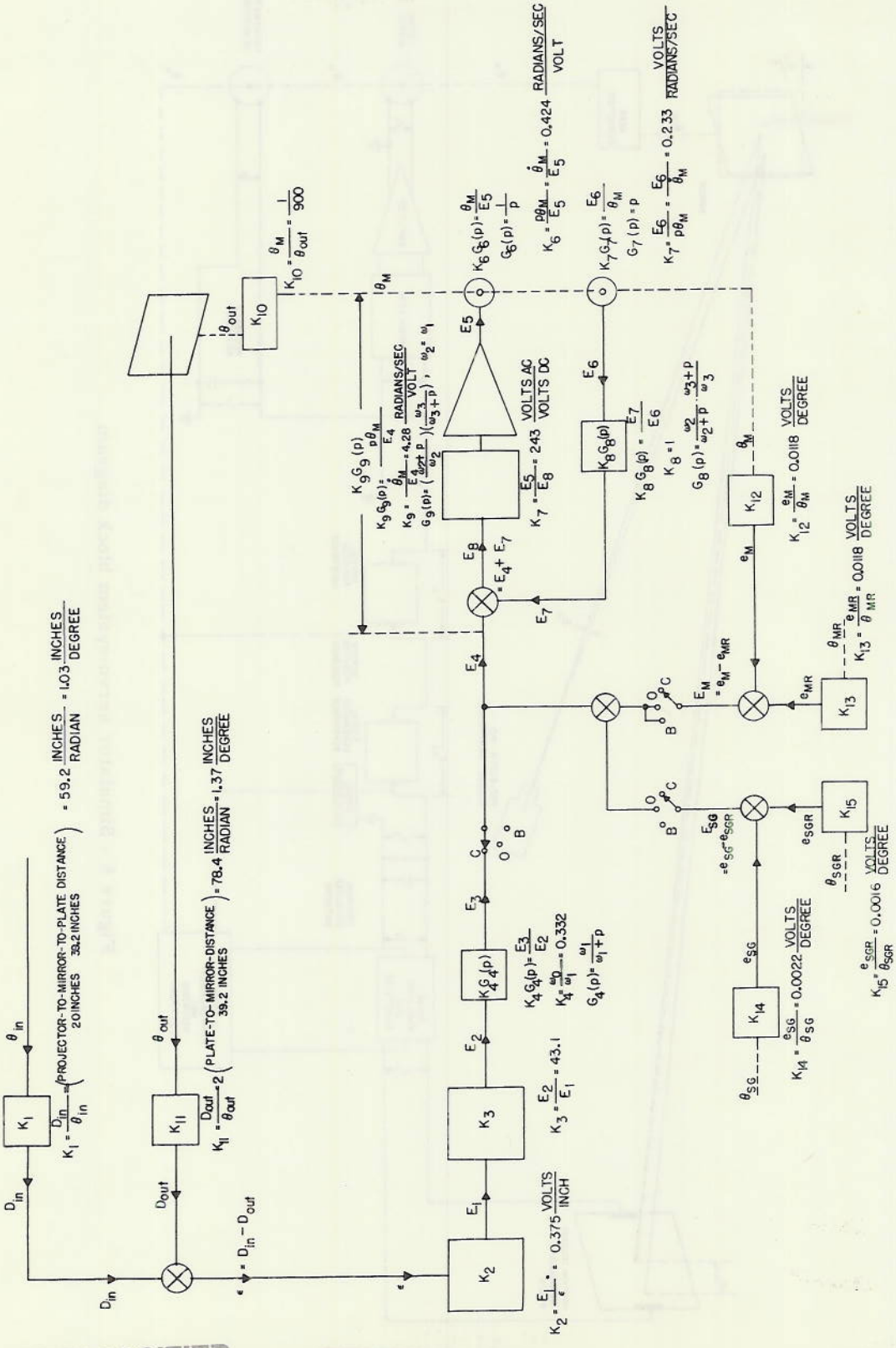

Figure 7 - Simulator servo-system functional diagram

THE PROJECTOR-MIRROR-PLATE FUNCTIONS

As previously described in a general way, the light patterns projected by reflection from the mirror form images at the plate that are tracked by the operating subject. Under perfect tracking any deflection of the image is compensated for with a return to and maintenance of a center of plate position of the image.

The geometry of the projector-mirror-plate system, for an input angle θ_{in} introduced at the projector, is given in Figure 8(a). The projector is located at the point P and the initial position of the mirror is the line SR. The initial ray of light from the projector is shown by the lines a and b with the image center at the plate indicated by 0. When the projector is turned through the angle θ_{in}, the reflection point moves from R to S and the image moves to the deflected position 0′. A compensating mirror angle θ_{out} results in a new reflection point T and a return of the image center to the initial plate position 0. Figure 8(b) shows the geometry of the system involved in conversion of an angular input signal θ_{in} into an essentially linear deflection of the image center from 0 to 0′. The projector is shown at its equivalent image position, P′. Let

a = initial projector-to-mirror distance,

b = initial mirror-to-plate distance, and

θ_{in} = angle through which projector is turned.

For the initial light ray normal to the plate (angle at 0 a 90° angle), the new angle at 0′ is seen to be 90° minus θ_{in}. Denoting the distance 00′ by D_{in} and using the law of sines, we may write

$$\frac{D_{in}}{\sin \theta_{in}} = \frac{a + b}{\sin (90^\circ - \theta_{in})}, \tag{29}$$

$$D_{in} = (a + b) \tan \theta_{in}, \text{ and}$$

$$\frac{D_{in}}{\theta_{in}} \doteq (a + b). \tag{30}$$

The approximation involved in Equation (30) introduces negligible error since θ_{in} does not exceed 2° in the actual equipment. In the system, a = 20 inches and b = 39.2 inches with the result

$$\frac{D_{in}}{\theta_{in}} = K_1 = 59.2 \frac{\text{inches}}{\text{radian}} = 1.03 \frac{\text{inches}}{\text{degree}}, \tag{31}$$

as shown in Figure 7.

The geometry for determination of the angular output to angular input ratio is given by Figure 9. Let

R = center of mirror rotation,

0 = image center on plate,

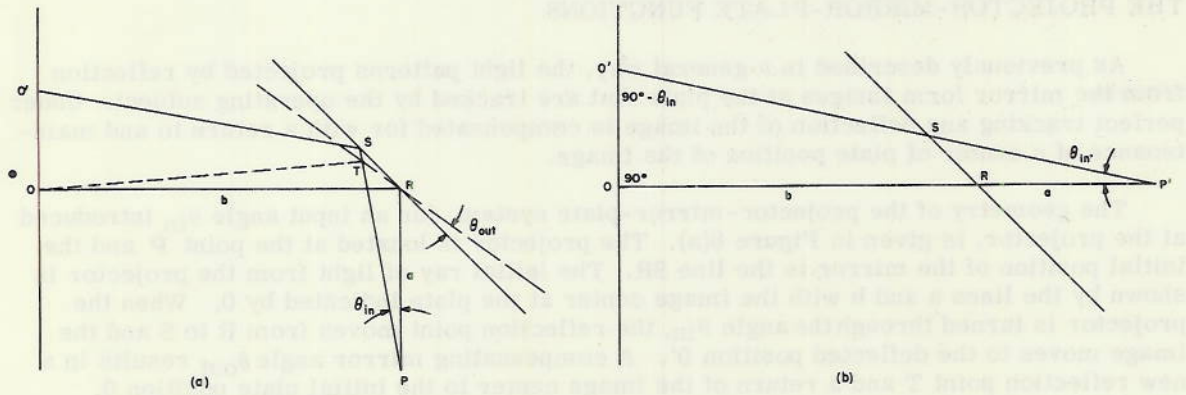

Figure 8 - (a) Geometry of projector-mirror-plate combination
(b) Diagram for angular input to linear deflection conversion

P = projector location,

a = initial projector-to-mirror distance,

b = initial mirror-to-plate distance,

θ_{in} = input angle at projector,

ϕ = initial angle of incidence, and

θ_{out} = compensating angular motion of mirror.

Using the law of sines and the triangle PRS of Figure 9(a), we may write

$$\frac{a}{\sin(\phi - \theta_{in})} = \frac{c}{\sin \theta_{in}} . \tag{32}$$

Using triangle URS and recognizing that

$$\sin\left[180^\circ - (2\phi - \theta_{in})\right] = \sin(2\phi - \theta_{in}),$$

we have

$$\frac{c}{\sin(2\phi - \theta_{in})} = \frac{d}{\sin(\phi - \theta_{in})} . \tag{33}$$

Solving Equations (32) and (33) simultaneously,

$$d = a \frac{\sin \theta_{in}}{\sin(2\phi - \theta_{in})} . \tag{34}$$

When the mirror is moved through a compensating angle, θ_{out}, the conditions are those shown in Fibure 9(b). Using triangle URT and recognizing that

$$\sin\left[180^\circ - (2\phi - \theta_{in})\right] = \sin(2\phi - \theta_{in}),$$

we may write

$$\frac{d}{\sin(\phi - \theta_{in} + \theta_{out})} = \frac{e}{\sin(2\phi - \theta_{in})} . \tag{35}$$

Substituting the value for d given by Equation (34) into Equation (35), we obtain

$$e = a \frac{\sin \theta_{in}}{\sin(\phi - \theta_{in} + \theta_{out})} . \tag{36}$$

Using triangle ORT, and recognizing that

$$\sin\left[180^\circ - (2\phi - 2\theta_{in} + 2\theta_{out}) + \phi - \theta_{in} + \theta_{out}\right] = \sin\left[\phi - \theta_{in} + \theta_{out}\right],$$

we have

$$\sin \frac{b}{(\phi - \theta_{in} + \theta_{out})} = \frac{e}{\sin(2\theta_{out} - \theta_{in})},$$

from which

$$e = b \frac{\sin(2\theta_{out} - \theta_{in})}{\sin(\phi - \theta_{in} + \theta_{out})} . \tag{37}$$

Equating (37) and (36),

$$b \frac{\sin(2\theta_{out} - \theta_{in})}{\sin(\phi - \theta_{in} + \theta_{out})} = a \frac{\sin \theta_{in}}{\sin(\phi - \theta_{in} + \theta_{out})} . \tag{38}$$

Equation (38) reduces as follows:

$$\sin(2\theta_{out} - \theta_{in}) = \frac{a}{b} \sin \theta_{in},$$

$$2\theta_{out} - \theta_{in} = \sin^{-1}\left(\frac{a}{b} \sin \theta_{in}\right),$$

$$\frac{\theta_{out}}{\theta_{in}} = \frac{1}{2} + \frac{1}{2\theta_{in}} \sin^{-1}\left(\frac{a}{b} \sin \theta_{in}\right). \tag{39}$$

For θ_{in} small (in the equipment θ_{in} does not exceed 2°), the $\sin \theta_{in} \doteq \theta_{in}$.

Then,

$$\frac{\theta_{out}}{\theta_{in}} = \frac{1}{2} + \frac{1}{2\theta_{in}} \left(\frac{a}{b} \theta_{in}\right),$$

and

$$\frac{\theta_{out}}{\theta_{in}} \doteq \frac{a + b}{2b} . \tag{40}$$

For a = 20 inches and b = 39.2 inches,

$$\frac{\theta_{out}}{\theta_{in}} = \frac{20 + 39.2}{2 \cdot 39.2} = 0.75. \tag{41}$$

The value for K_{11} given in Figure 7 is obtained by recognizing that $D_{out} = D_{in}$ for zero error; i.e., for perfect compensatory response. Accordingly, using the values given by Equations (31) and (41),

$$K_{11} = \frac{D_{out}}{\theta_{out}} = \frac{K_1 \theta_{in}}{\theta_{out}} = \frac{59.2}{0.75},$$

$$K_{11} = \frac{D_{out}}{\theta_{out}} = 2b = 78.4 \frac{\text{inches}}{\text{radian}} = 1.37 \frac{\text{inches}}{\text{degree}}. \tag{42}$$

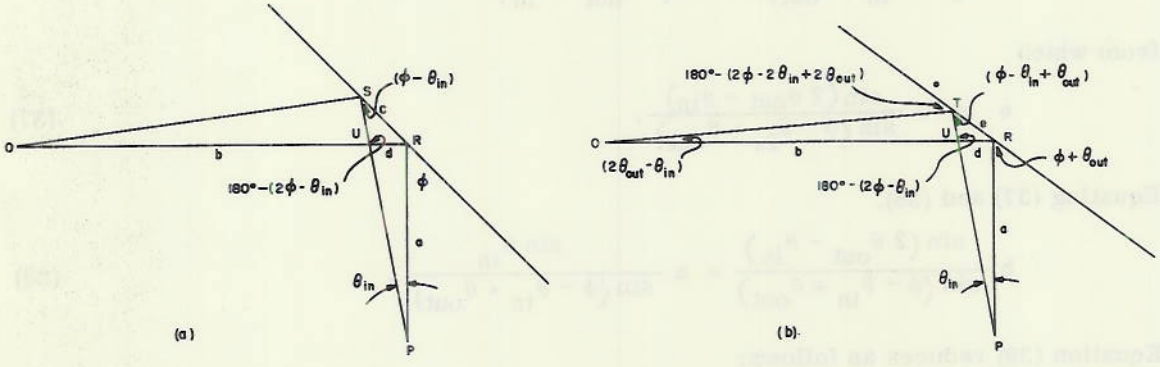

Figure 9 - Geometry for determination of angular output to angular input ratio
(a) Mirror in initial position
(b) Mirror in compensating position

The projector-mirror-plate mechanism is thus seen to provide a projector-angular-input to plate-image-deflection conversion gain of 1.03 inches per degree and a mirror-angular-output to compensatory plate-image-deflection conversion gain of 1.37 inches per degree for a projector-to-mirror distance of 20 inches and a mirror-to-plate distance of 39.2 inches. It should be noted that a simple means for adjusting the frequency bandpass of the missile simulator servo system is adjustment of the conversion gain K_{11} by changing the distance b (the mirror-to-plate distance). The input signal characteristics are unchanged provided a compensating change is made in the distance a (i.e., keeping the value of a + b constant). If it is desired to change the angular rates produced by the cam that controls the projector angular position without changing the system gain, only the distance a need be changed.

THE POSITION-VOLTAGE TRANSDUCER PLATE

The target image as projected by reflection from the mirror appears on the ground-glass surface of a square glass plate. This same surface is coated with a thin, baked-on,

conducting, film of stannic oxide. Electrode strips are formed at each edge by a silver-evaporation process. For the 12-inch square plate used, the electrodes were made approximately 1/2 inch by 6 inches in size. Figure 10 shows one pair of the electrodes and the associated resistance bridge circuit. The magnitude of the voltage difference appearing at a pair of plate electrodes, under probe in contact conditions, is taken as a direct measure of probe position. The operating subject's upper beak is equipped with a small silver tip which has a flexible connection to system (and earth) ground potential. It is considered good practice to arrange the circuit so that a grounded probe is involved. Note that no current flows except when the probe is in contact with the plate. The bridge resistance, designated by R_c and R_d in Figure 10, are made equal to approximately one-half of the plate electrode-to-electrode resistance for greatest bridge sensitivity.

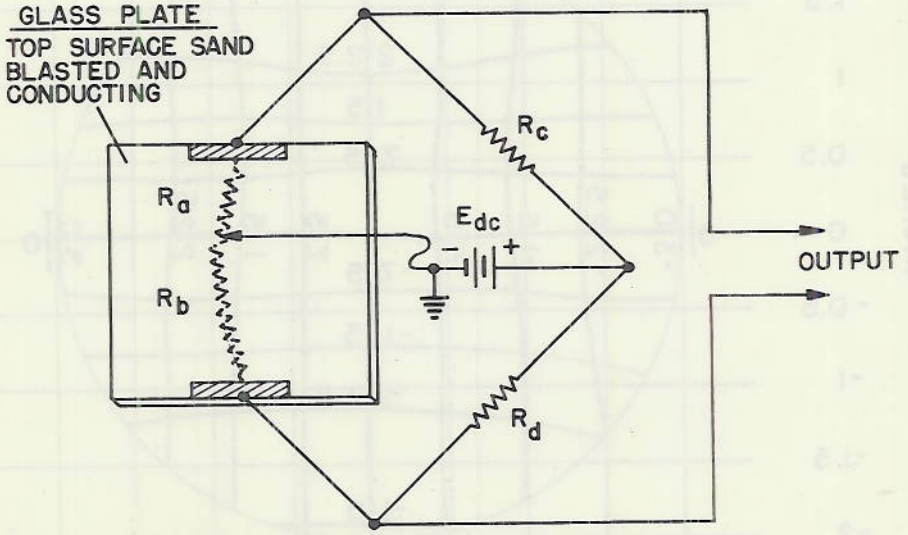

Figure 10 - Position-voltage transducer

A field map of the voltage output of the pulse stretcher as a function of position was made for a particular plate with measurements of both left-right and up-down signals made on a 1/2-inch grid over the central 4-inch-diameter region exposed to the operating subject. Figure 11 shows the resulting pattern to be of a reasonably linear nature. Deviations from perfect linearity have little significance in the servo system operation but cause considerable difficulty in automatic scoring equipment developed for continuous monitoring and reinforcement-by-rewarding during the training of the operating subjects. During research work with the system, careful plate selection and periodic plate condition checks were made because of this nonlinearity.

A check of a plate alone yields the value K_2 = 0.375 volts per inch for the position-voltage-transducer gain as given on Figure 7.

The nature of the voltage pulses obtained with an operating subject were investigated by means of high-speed photography of the pulse-amplifier output. Figure 12 shows some typical results. From the standpoint of the missile simulator servo system, a simple

acceptance of the entire wave train for a pulse-stretcher input signal is entirely adequate. However, the training of an operating subject was to be accomplished by an automatic, continuous monitoring of each pulse on a hit-or-miss basis. When sufficient hits are accumulated, a reward mechanism is operated. Such a requirement demands that only a single portion of each wave train be sampled and used in such equipment. A study of the wave trains leads to the conclusion that the initial leading edge of the wave is probably the only portion that could be used in automatic equipment. The wide variability of a well-trained, good-performing subject is shown in Figure 12 and by Table 5.

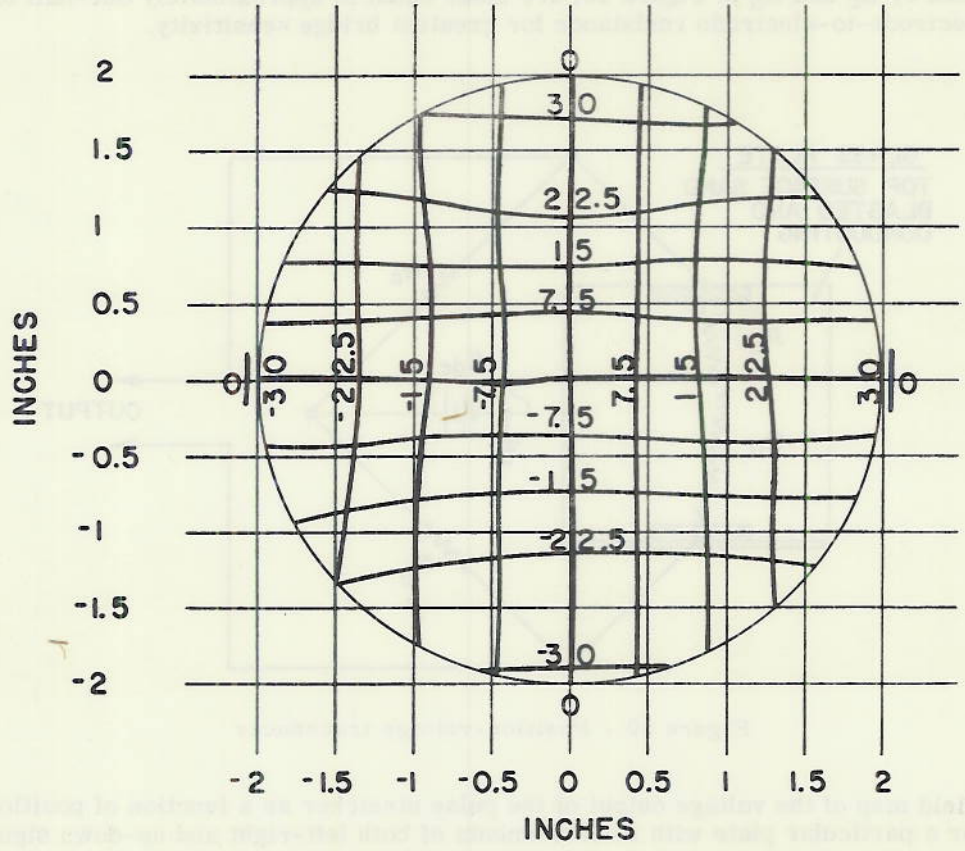

Figure 11 - Field map of transducer plate voltage measured at pulse stretcher output

The factors (a) duration of initial contact, (b) duration of interval between contacts, (c) duration of second contact, and (d) pecks per second were considered with a view of establishing specifications for a gating circuit. The gating circuit must operate to take as short a sample as possible with a minimum of delay from the leading edge. All subsequent information must be rejected without imposing a severe limit to the frequency of the incoming intelligence (e.g., response to 10 pecks per second is desired). In particular, it is very necessary that a final voltage spike at the end of a waveform should not cause the sampling of the immediately subsequent zero voltage and thus indicate an extraneous zero-center or no-error peck.

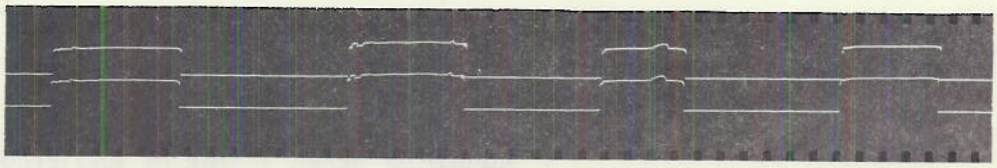

(a) GAIN CALIBRATION USING NEEDLE PROBE—SAME VOLTAGE ON BOTH CHANNELS.

(b) SINGLE PULSE GROUP, 2.9 MILLISECONDS, DECREASING AMPLITUDE, NO CONTACT BOUNCE.

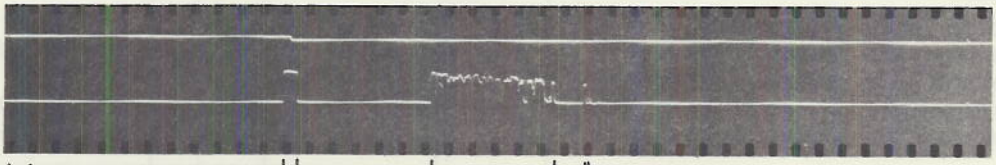

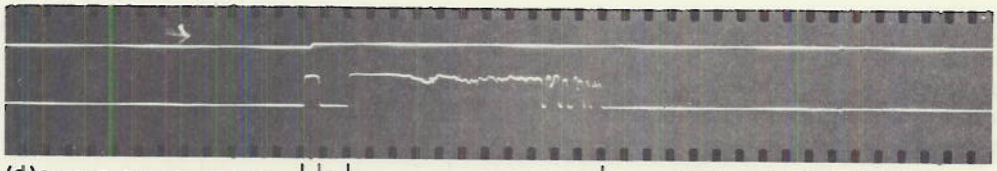

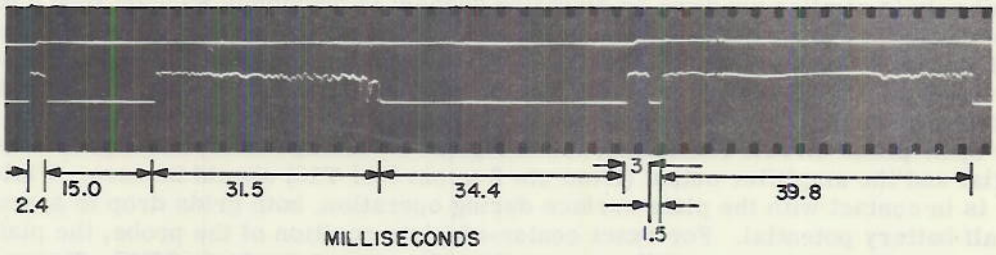

(e) TWO PULSE GROUPS WITH CONTACT BOUNCE—EACH GROUP SAMPLED ONCE.

Figure 12 - Pulse waveforms from high-speed photography of oscillograph at amplifier output under typical conditions. Upper trace of (b) through (e) strips shows pulse stretcher output.

[redacted]

TABLE 5
Pulse Characteristics from High-Speed Photography of Oscillograph at Amplifier Output under Typical Conditions

	NUMBER OF PECKS		TIME IN MILLISECONDS		
	TOTAL	NO BOUNCE	MINIMUM	MAXIMUM	AVERAGE
SUBJECT #3, 1st SESSION	35	5			
DURATION OF INITIAL CONTACT			1.5	4.5	2.98
DURATION OF INTERVAL BETWEEN CONTACTS			3.25	11.5	8.45
DURATION OF SECOND CONTACT			15.0	44.5	24.88
SUBJECT #10, 1st SESSION	52	0			
DURATION OF INITIAL CONTACT			1.65	3.0	2.05
DURATION OF INTERVAL BETWEEN CONTACTS			2.5	19.5	9.75
DURATION OF SECOND CONTACT			12.0	44.5	25.09
SUBJECT #10, 2nd SESSION	28	5			
DURATION OF INITIAL CONTACT			2.0	3.0	2.49
DURATION OF INTERVAL BETWEEN CONTACTS			2.0	9.5	6.33
DURATION OF SECOND CONTACT			20.0	42.0	31.98

THE PULSE AMPLIFIER AND STRETCHER

A complete schematic diagram of the pulse amplifier and stretcher unit is given in Figure 13. The unit has the position-voltage transducer plate circuitry at the input and provides outputs to the servo system and to the recording and scoring equipment. The functional diagram given in Figure 14 is helpful in a discussion of the operation of the unit, which includes a total of twenty-one tubes.

The signals from each electrode of the transducer plate are with respect to ground potential. Consequently, a differential amplifier is used. This double-ended circuitry is carried through to the modulator. If the signal is traced through the left-right or train channel only (a similar up-down or elevation channel is provided), vacuum tube V16 together with V11 in its cathode circuit is seen to be the only amplifying stage. The portion of Figure 13 involved here, given in Figure 15, is the balanced amplifier and the point from which a gating signal is derived. The problem of stability of balance is effectively eliminated by the use of the large value of common cathode impedance provided by V11. Under open-probe circuit conditions, the two grids of V16 are at identical (full battery) potential and the amplifier output (from pin 2 to pin 5 of V16) should be zero. While the probe is in contact with the plate surface during operation, both grids drop to approximately one-half battery potential. For exact center-of-plate position of the probe, the plate bridge circuitry is adjusted for zero difference voltage from pin 1 to pin 4 of V16. Under this balanced input, the amplifier output should be zero. The particular amplifier circuit shown maintains balance over the necessary range (i.e., has negligible "common mode effect"). For the probe off-center, a difference potential develops and appears as an amplified output signal simultaneous with a drop in potential at the plate of V11. The magnitude of the signal at the plate of V11 is proportional to the average of the grid potentials and, accordingly, is essentially independent of the probe position. It is thus seen that the signal at pin 8 of V11 is excellently suited for gating and is so used.

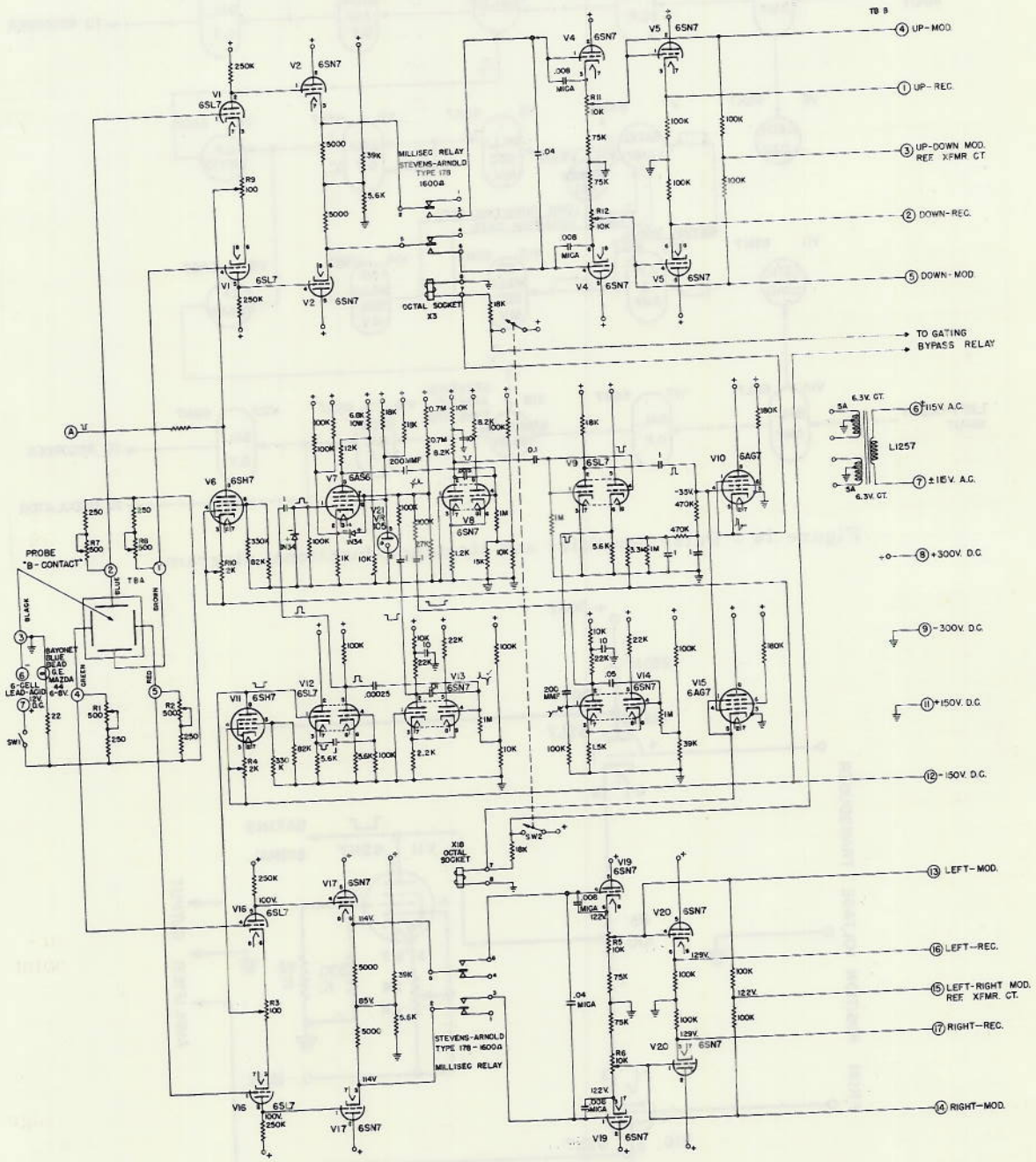

Figure 13 - Pulse amplifier and stretcher-schematic diagram

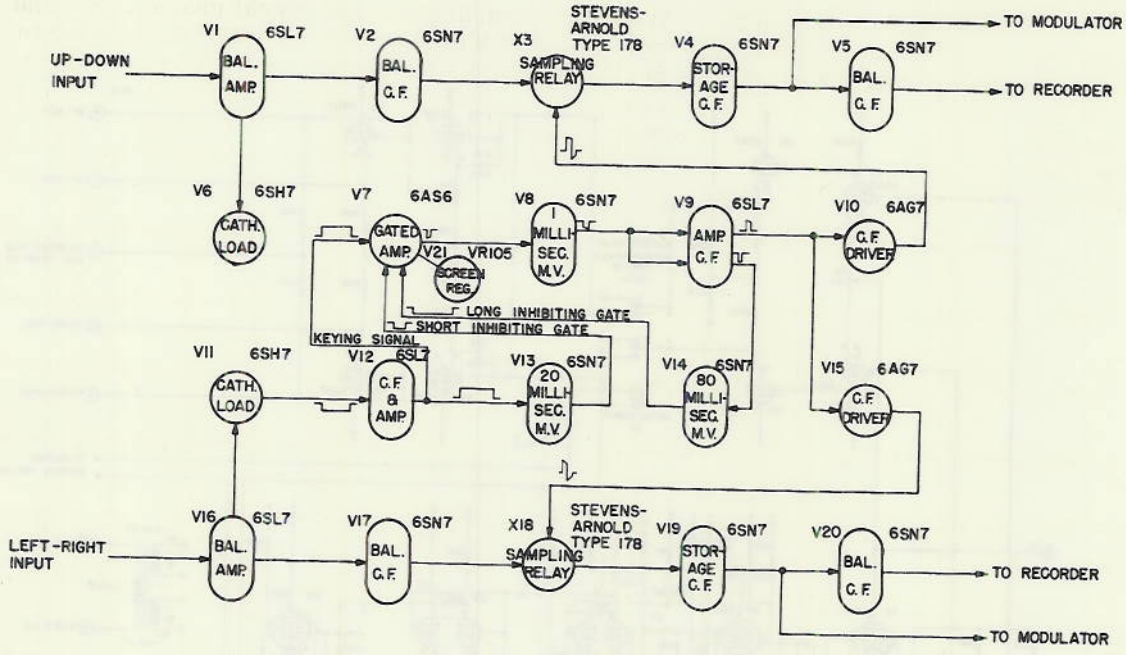

Figure 14 - Pulse amplifier and stretcher-functional diagram

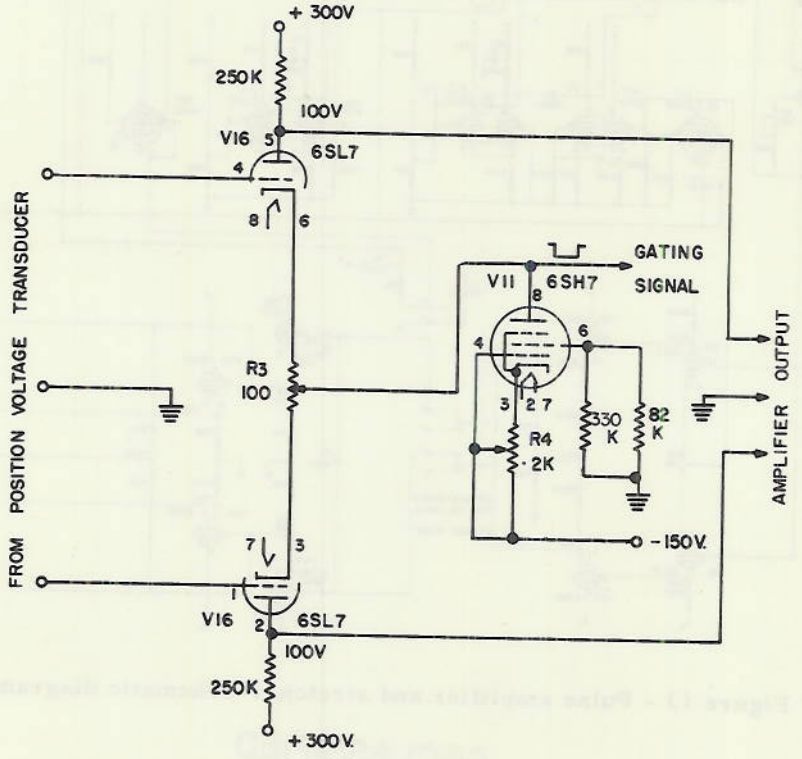

Figure 15 - Pulse amplifier and gating signal source

By switching SW2 (see Figure 13) closed, measurements of signal channel gain and linearity including the cathode followers V17, and V19 may be made (V20 is included in measurements of the output to recorders). The results given in Figure 16 were obtained from an average of pulse amplitudes. The pulses were generated by operating a switch inserted in the probe lead while the probe was accurately positioned on the plate. From the slope, the gain is found to agree with the much later measurement of $K_3 = 43.1$ given in Figure 7.

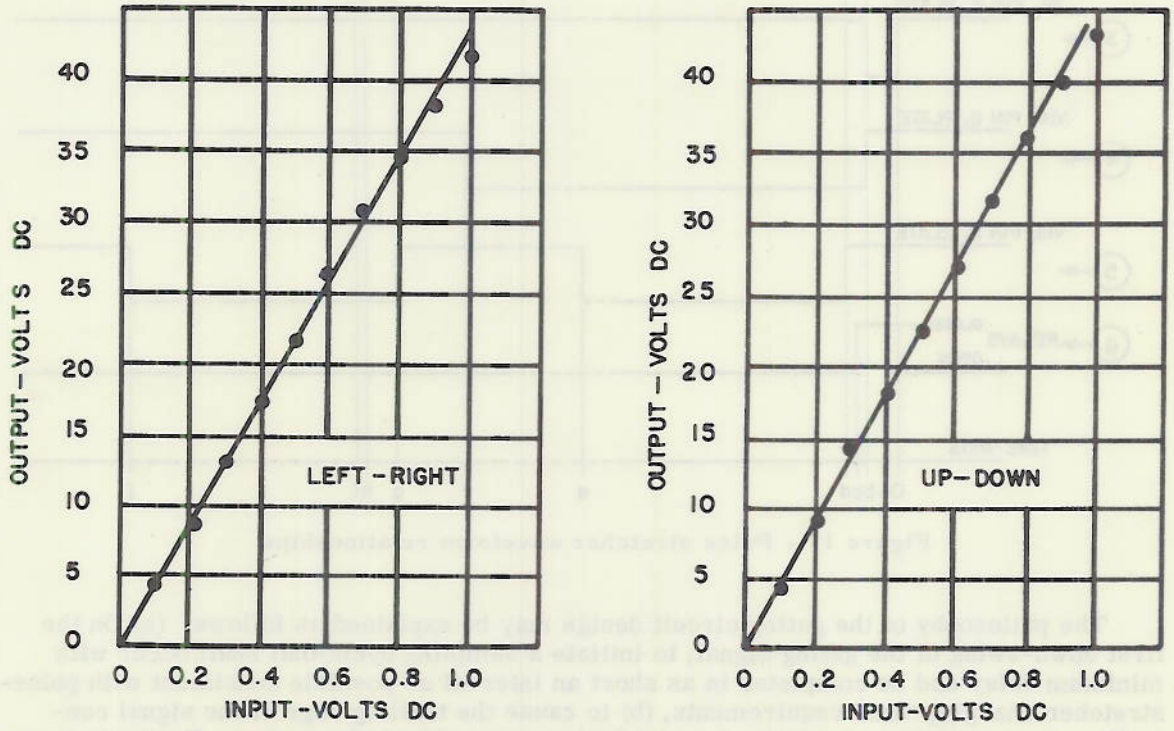

PROBE POSITION ON TRANSDUCER PLATE HELD CONSTANT AND CIRCUIT INTERRUPTED TO OBTAIN AVERAGE OUTPUT UNDER DYNAMIC PULSE STRETCHER CONDITIONS.

Figure 16 - Pulse amplifier-stretcher signal channel linearity verification

From a study of the pulse waveforms obtained with operating subjects (examples given in Figure 12 and summary given in Table 5), a prototype waveform was formulated. It was recognized that less than 100% performance could be expected regardless of the complexity of the prototype waveform selected and of the gating circuitry evolved. The occurrence of an occasional faulty sampling in actual operation has little effect on the servo-system operation but directly effects the continuous scoring upon which the operating subject's rewarding (called reinforcement) is based. The ultimate measure of success or failure of a given design was recognized to be related to the ability to train the operating subject. If training is accomplished in a reasonable time, the particular design may be termed acceptable. The form of the prototype waveform used in the design of the equipment described here is shown by the negative gating signal appearing at V11-pin 8-plate, as illustrated by waveform 1 of Figure 17.

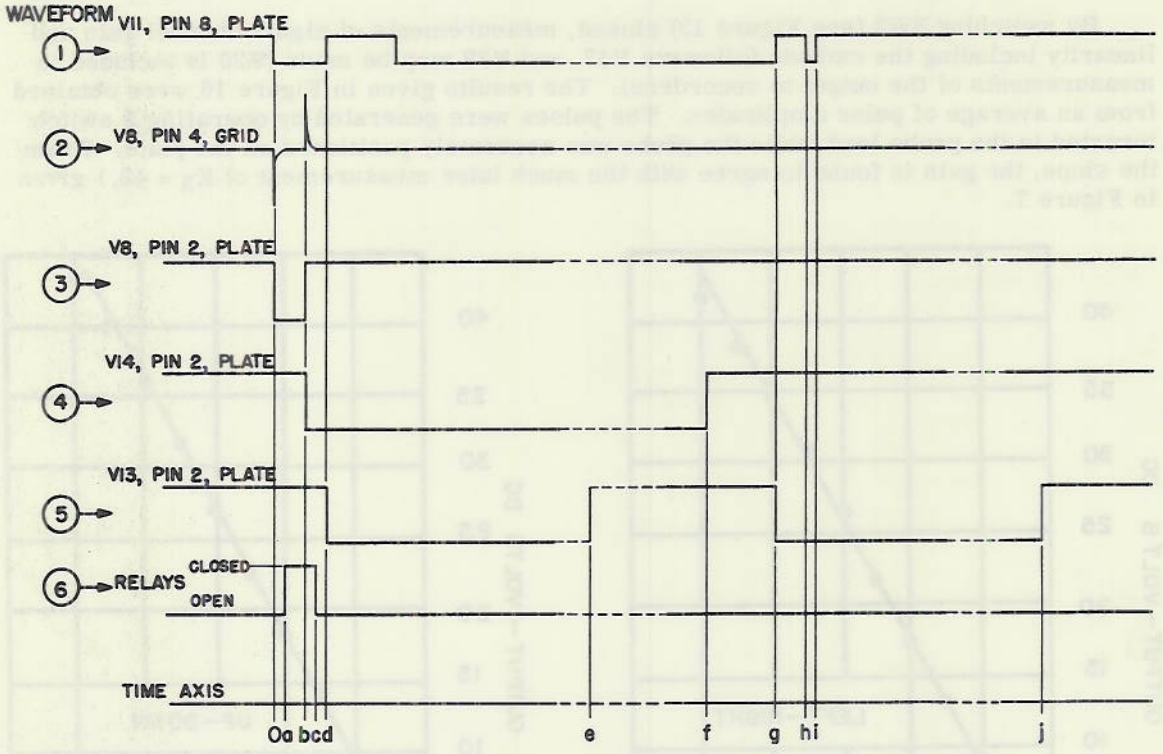

Figure 17 - Pulse stretcher waveform relationships

The philosophy of the gating circuit design may be explained as follows: (a) On the first down-swing of the gating signal, to initiate a sampling cycle that shall occur with minimum delay and be completed in as short an interval as possible consistent with pulse-stretcher charging-time requirements, (b) to cause the trailing edge of the signal controlling the sampling to initiate a long inhibiting gate to block the system effectively from subsequent triggering by later gating-signal down-swings, and (c) on the first up-swing of the gating signal (corresponding to a signal drop-out), to initiate a short inhibiting gate. The presence of either or both of the short or long inhibiting-gate signals prevents sampling. A study of Figure 17 and Figure 14 reveals the manner in which the foregoing objectives are accomplished. The time interval Ob is reduced to approximately 1 millisecond by the circuit constants employed in the V8 multivibrator. The interval ac (equal in duration to Ob) occurs with approximately a 0.2 millisecond delay owing to the electromechanical-relay time delay. Note that the gating signal is blocked during the interval bc. This has no effect on the signal sampled since the sampling-relay contacts are in series with the signal channel (not the gating signal path). The long inhibiting gate is set at 80 milliseconds by the V14 multivibrator and the short inhibiting gate is set at 20 milliseconds by a similar multivibrator V13. The gating and signal mixing functions are accomplished by the circuits of V7 which are shown separately in Figure 18.

The one-millisecond pulse generated by the V8 multivibrator is coupled through the V9 cathode follower and applied to the relay driver cathode followers V10 and V15 (Figure 19 shows the circuit schematic). The 1600-ohm relay coil is rated at 24 volts. By subjecting the relay to a 35-volt square pulse, the relay closing time delay was reduced to approximately 0.2 millisecond with no contact chatter on make or break. As shown on the over-all schematic of Figure 13 and on the pulse-stretcher detail schematic, Figure 20,

the normally open contacts of the relay are connected to the grids of V19 and a 0.04-μfd mica condenser is connected from grid to grid. Under normal tracking conditions, the amplitude of successive pulses is a slowly varying function. The differential charging circuit (shown in Figure 20) has the advantage of not charging from zero on each pulse, with the result that errors due to short charging time are a second-order effect. Since the charging source is disconnected after a one-millisecond sample of pulse amplitude, an extremely long discharge time-constant is obtained. This characteristic is especially important during early training where pauses between pecks of 2 minutes duration sometimes occur. The output is taken from potentiometer taps so that a final adjustment of output balance and of gain balance between channels may be made.

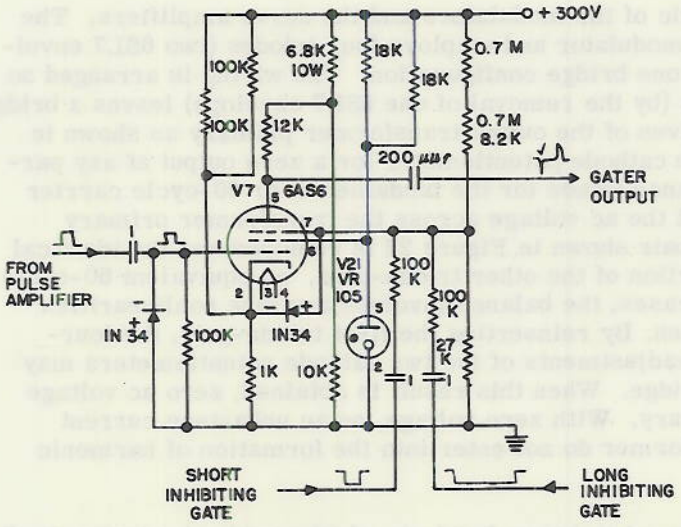

Figure 18 - Gating amplifier schematic

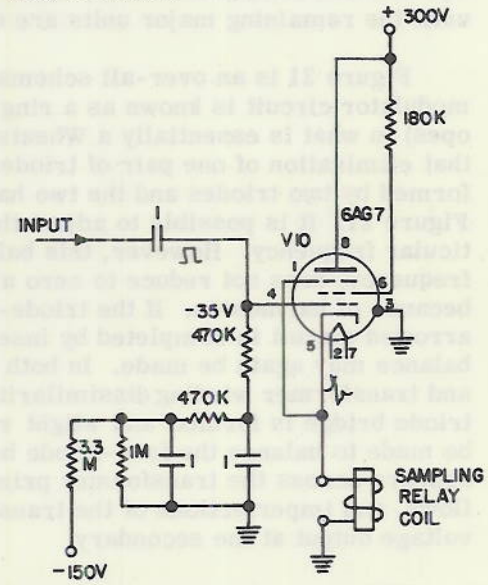

Figure 19 - Relay driver schematic

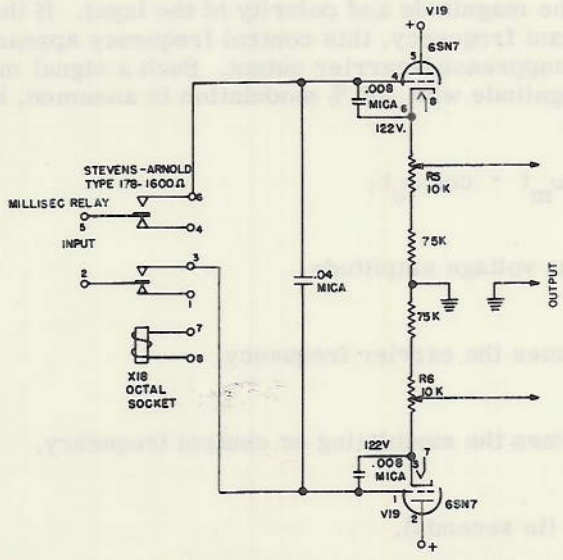

Figure 20 - Pulse stretcher schematic

Signals to the recording and scoring equipment are provided at TB B-1 and B-2 for up-down and TB B-16 and B-17 for left-right (see Figure 12). The occurrence of a peck is signalled by the negative gate brought to the external connection TB A-A.

THE MODULATOR AND SERVO AMPLIFIER

Figure 6 shows considerable circuitry between the pulse amplifier-stretcher unit and the modulator. Since much of this portion of the equipment is related to servo system equalization control and to the mode-of-operation control, the description will be delayed until the remaining major units are discussed.

Figure 21 is an over-all schematic of the modulators and the servo amplifiers. The modulator circuit is known as a ring modulator and employs four triodes (two 6SL7 envelopes) in what is essentially a Wheatstone bridge configuration. The wiring is arranged so that elimination of one pair of triodes (by the removal of one 6SL7 envelope) leaves a bridge formed by two triodes and the two halves of the output transformer primary as shown in Figure 21. It is possible to adjust the cathode potentiometer for a zero output at any particular frequency. However, this balance (made for the fundamental or 60-cycle carrier frequency) does not reduce to zero all the ac voltage across the transformer primary because of harmonics. If the triode-pair shown in Figure 22 is removed and the identical arrowed circuit is completed by insertion of the other triode-pair, an equivalent 60-cycle balance may again be made. In both cases, the balance involves any tube nonlinearities and transformer winding dissimilarities. By reinserting the first triode-pair, the four-triode bridge is formed and slight readjustments of the two cathode potentiometers may be made to balance the four-triode bridge. When this result is obtained, zero ac voltage appears across the transformer primary. With zero voltage, no ac unbalance current flows, and imperfections of the transformer do not enter into the formation of harmonic voltage output at the secondary.

With the modulator properly balanced and zero input signal (the grids short-circuited), no voltage appears at the modulator output. When an input dc unbalance is applied (i.e., under steady input signal conditions), a 60-cycle voltage is developed with amplitude and phase determined by the magnitude and polarity of the input. If the input signal varies sinusoidally at a constant frequency, this control frequency appears as the envelope frequency of a 60-cycle suppressed-carrier output. Such a signal may be described mathematically, if a unit magnitude with 100 % modulation is assumed, by the equation

$$e = \cos \omega_m t \cdot \cos \omega_o t, \tag{43}$$

where e = instantaneous voltage amplitude,

ω_o = 2π times the carrier frequency,

ω_m = 2π times the modulating or control frequency,

and t = time (in seconds).

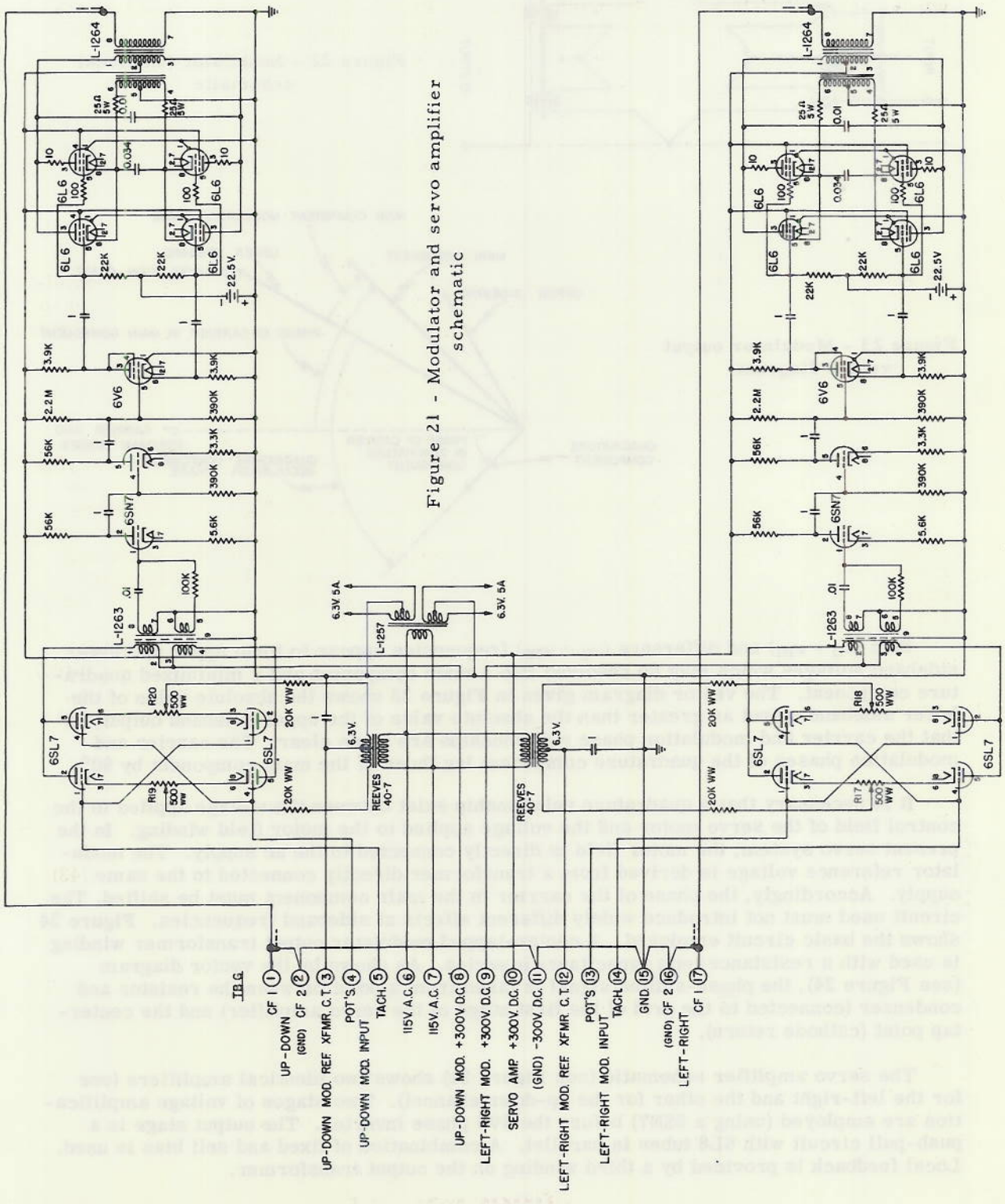

Figure 21 - Modulator and servo amplifier schematic

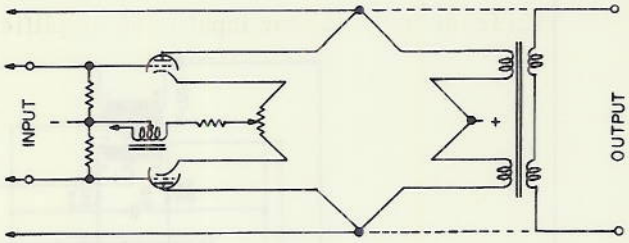

Figure 22 - Modulator functional schematic

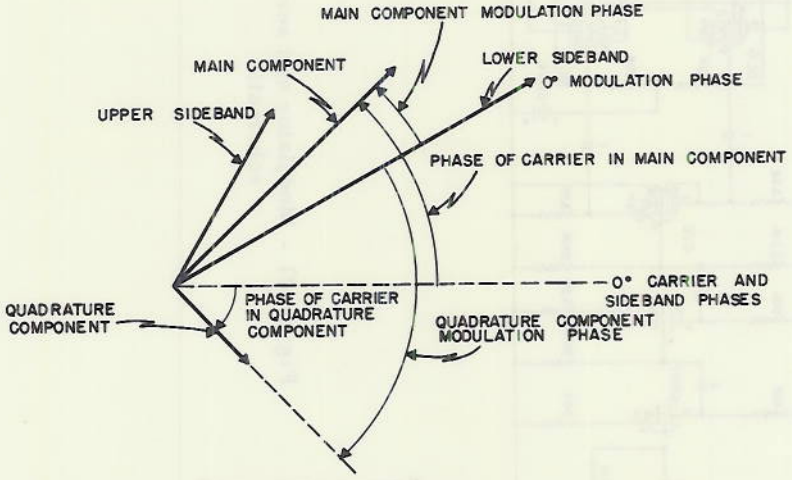

Figure 23 - Modulator output vector diagram

Sum ($\omega_0 + \omega_m$) and difference ($\omega_0 - \omega_m$) frequencies appear to form upper and lower sideband voltages which may be resolved into a main component and a minimized quadrature component. The vector diagram given in Figure 23 shows the absolute value of the lower sideband output as greater than the absolute value of the upper sideband output, so that the carrier and modulation phase relationships are made clear. The carrier and modulation phases of the quadrature component lag those of the main component by 90°.

It is necessary that a quadrature relationship exist between the voltage applied to the control field of the servo motor and the voltage applied to the motor field winding. In the present servo system, the motor field is directly connected to the ac supply. The modulator reference voltage is derived from a transformer directly connected to the same supply. Accordingly, the phase of the carrier in the main component must be shifted. The circuit used must not introduce widely different effects at sideband frequencies. Figure 24 shows the basic circuit employed. A center-tapped modulator output transformer winding is used with a resistance and a capacitance in series. As shown by the vector diagram (see Figure 24), the phase-shifted signal is taken from a point between the resistor and condenser (connected to the grid of the first stage of the servo amplifier) and the center-tap point (cathode return).

The servo amplifier schematic (see Figure 21) shows two identical amplifiers (one for the left-right and the other for the up-down channel). Two stages of voltage amplification are employed (using a 6SN7) before the 6V6 phase inverter. The output stage is a push-pull circuit with 6L6 tubes in parallel. A combination of fixed and self bias is used. Local feedback is provided by a third winding on the output transformer.

Performance tests revealed a conversion gain from dc modulator input to ac amplifier output of

$$K_7 = \frac{E_5}{E_8} = 243 \frac{\text{Volts AC}}{\text{Volts DC}} \tag{44}$$

as shown in Figure 7.

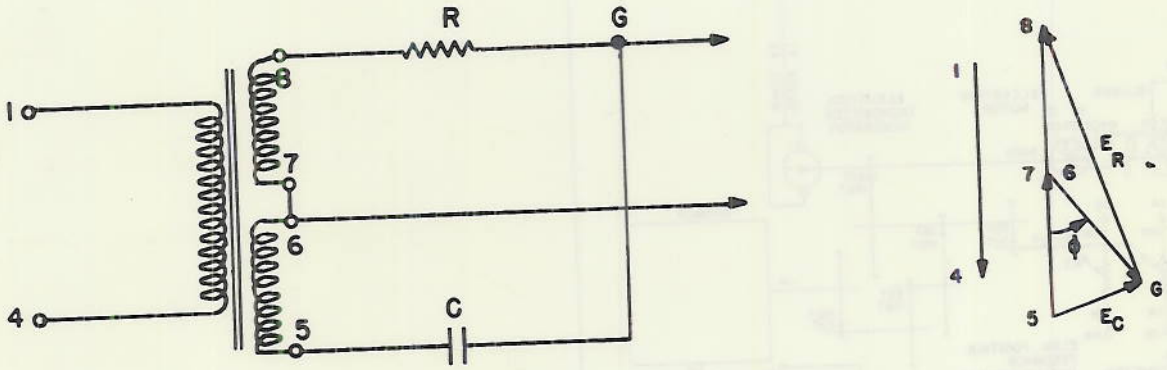

Figure 24 - Phase shifter schematic and voltage vector diagram

THE MIRROR MECHANISM

The mirror unit contains a front-surfaced mirror in a gear-driven universal mounting. Such a mounting has two degrees-of-freedom and, by proper orientation, these become left-right (train axis) and up-down (elevation axis) position control channels. A 900-to-1 gear reduction is incorporated between the servo control motors and the mirror. Figure 25 shows the electrical and the gearing details of the two-axis mirror mechanism. Instrument dc tachometer generators are directly coupled to the 900-speed motor shafts. These generators produce a voltage directly proportional to the rate of change of mirror position which is used as a servo system velocity feedback signal. Potentiometers, geared properly to sweep through approximately 9 turns of their 10-turn limit of rotation for a mirror angular deflection from limit-stop to limit-stop, produce a position monitoring signal (used in the scoring system) and a position feedback signal (used in the servo system during open-loop conditions).

System measurements (results shown in Figure 7) give a servo motor transducer gain

$$K_6 = 0.424 \frac{\text{radians/second}}{\text{volt}}, \tag{45}$$

a tachometer generator transducer gain

$$K_7 = 0.233 \frac{\text{volts}}{\text{radians/second}}, \tag{46}$$

and the previously mentioned gearing ratio

$$K_{10} = \frac{1}{900}. \tag{47}$$

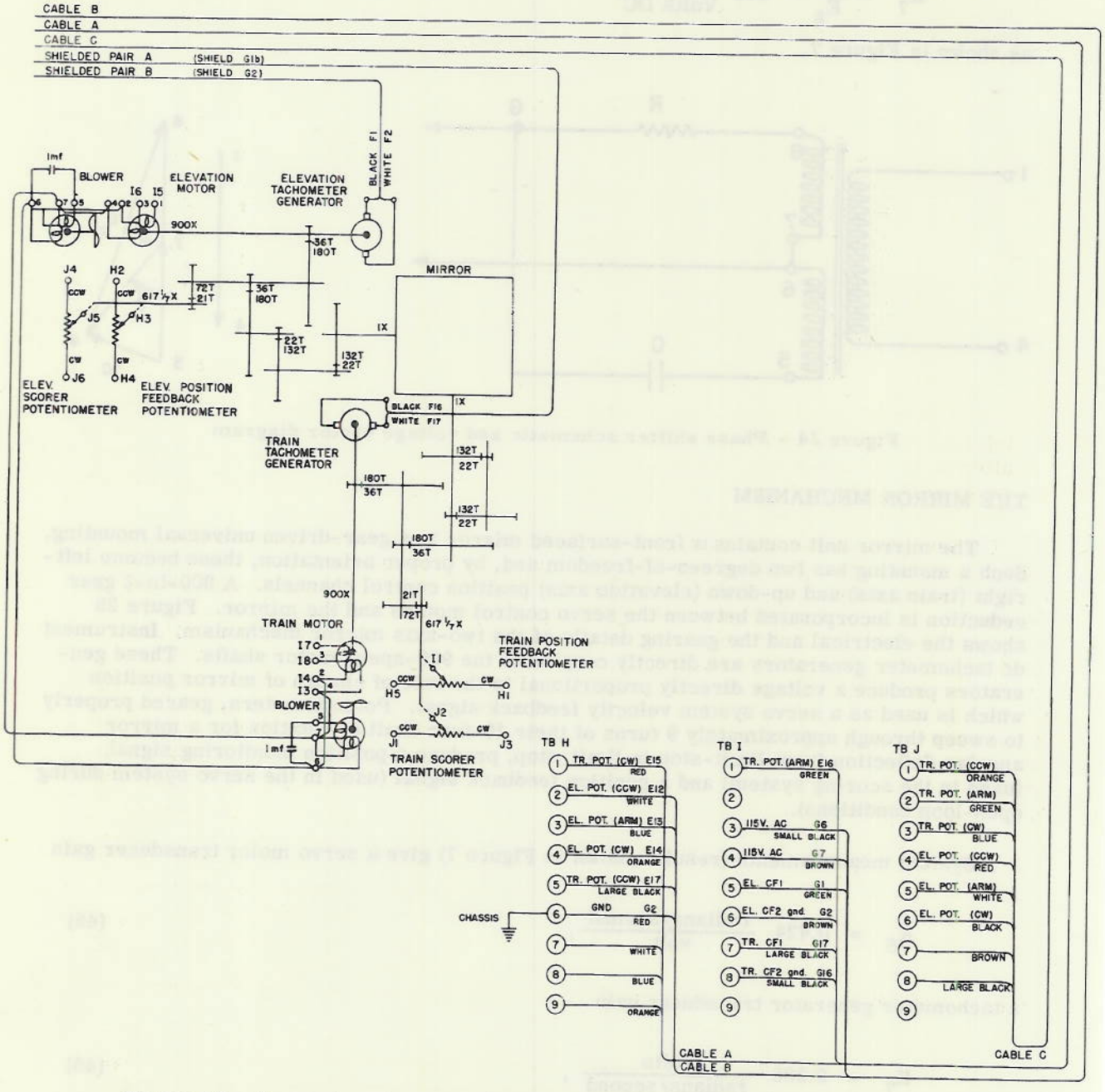

Figure 25 - Two-axis mirror mechanism gearing and electrical details

THE TACTICAL COURSE GENERATOR

As previously discussed, the tactical problem proposed for simulation is that of a pilotless aircraft or missile attacking a ship at sea moving along a straight line at constant speed. A projector angular-position-control cam is used to introduce the tracking problem into the system. The design of the cam is based on Flight Path 2 (shown in Figure 2) for which, repeating,

Target Ship Size: 100 yards in length,

Target Ship Speed: 20 yards/second,

Missile Speed: 300 yards/second,

Launching Position: 9000 yards abeam of target and 300 yards up-range,

Collision Range: 600 yards from target,

Range to Target after 28 Seconds of Flight: 608 yards.

Figure 26 shows the pursuit flight path of the attacking missile used as the basic information for the simulator tactical course cam design. Since the range to the target after 28 seconds of flight (608 yards) is essentially the same as the specified collision range of 600 yards, the course cam periphery is made to simulate the flight path no further than the 28-second point.

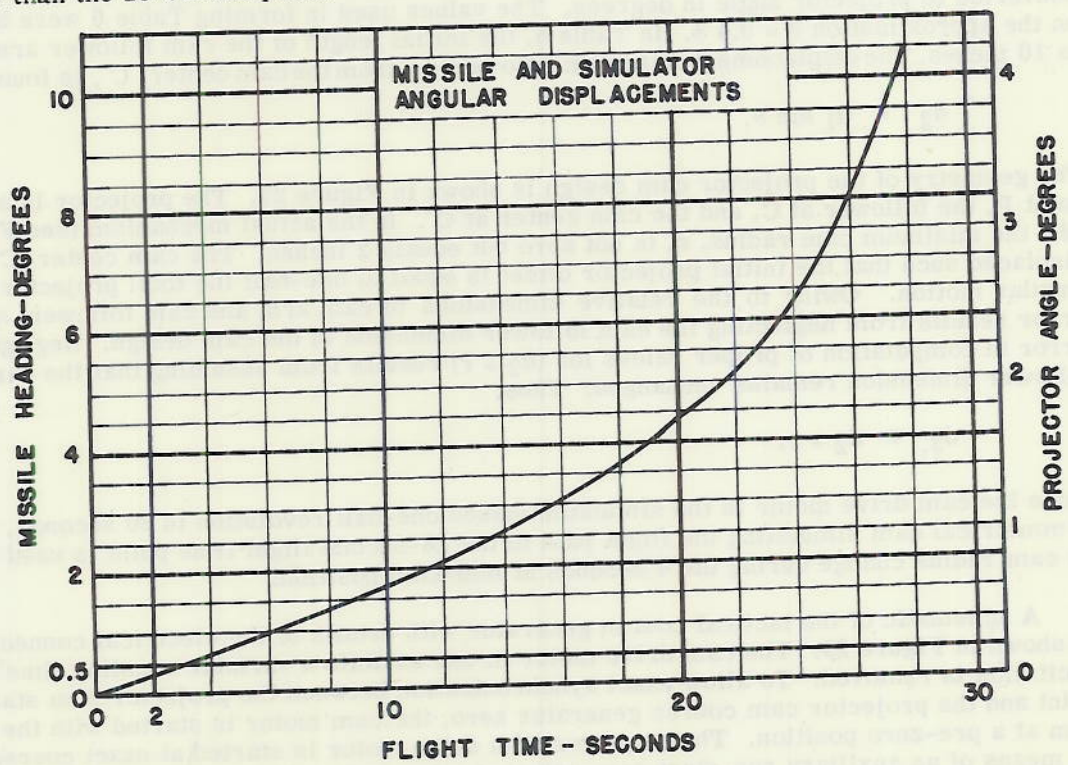

Figure 26 - Simulator design information for cam construction

The position-voltage transducer illustrated in Figure 10 has a working surface 4 inches in diameter which represents the operating subject's field of view. The target image is to extend from edge-to-edge (appear 4 inches in length) at collision range.

Using a projector-to-mirror-to-plate total distance of 20 + 39.2 = 59.2 inches and a 4-inch field of view, the equivalent angular field of view is

$$\theta = 2 \tan^{-1}\left(\frac{2}{59.2}\right) = 3.87 \text{ degrees.} \tag{48}$$

At the 28-second point the target must fill the field of view. Thus,

$$\phi = 2 \tan^{-1}\left(\frac{50}{608}\right) = 9.4 \text{ degrees.} \tag{49}$$

The ratio of θ divided by ϕ yields

$$\theta = 0.411\,\phi\,, \tag{50}$$

where

$\theta \equiv$ projector angular position, and

$\phi \equiv$ missile heading.

By using the conversion factor given in Equation (50), the missile heading in degrees is converted to projector angle in degrees. The values used in forming Table 6 were based on the approximation $\theta = 0.4\,\phi$. In Table 6, the initial length of the cam follower arm, d_1, is 10 inches. The displacement of the cam follower, d_2, from the cam center, C′, is found by

$$d_2 = d_1 \sin\theta. \tag{51}$$

The geometry of the projector cam design is shown in Figure 27. The projector is at the point P, the follower at C, and the cam center at C′. In the actual mechanism (see Figure 28), the minimum cam radius, r, is not zero but equals 2 inches. The cam center, C′, is displaced such that the initial projector offset is equal to one-half the total projector angular motion. Owing to the relative dimensions of cam arm and cam follower, small error results from neglecting the cam follower dimension in the cam design. Negligible error in computation of proper values for $(d_2 + r)$ results from assuming that the cam follower dimension remains unchanged. Thus,

$$d_3 \doteq d_2 + r. \tag{52}$$

Since the cam drive motor in the simulator makes one-half revolution in 30 seconds, a symmetrical cam simulating the flight path to the 28-second flight time point is used with no cam radius change during the 4 seconds at mid-cam position.

A schematic of the tactical course generator with details of the electrical connections is shown in Figure 29. The cam drive motor in use exhibits a variable coasting time after excitation is removed. To allow exact synchronization between the projector film starting point and the projector cam course generator zero, the cam motor is started with the course cam at a pre-zero position. The projector film drive motor is started at exact course zero by means of an auxiliary run-start cam-actuated microswitch (see Figure 29).

TABLE 6
Simulator Design Data for Tactical Problem

Time from Launching t (Seconds)	Missile Heading (Graphical) ϕ (Degrees)	Projector Angle ($\theta = 0.4\phi$) θ (Degrees)	$d_2 = d_1 \sin\theta$ (for $d_1 = 10''$) d_2 (Inches)	$d_3 = d_2 + r$ (for $r = 2''$) d_3 (Inches)	$\theta_{in} = \theta - \theta$ init. (for $\theta_{init.} = 2.122$) θ_{in} (Degrees)
0	0	0	0	2.000	-2.122
1	0.17	0.068	0.012	2.012	-2.054
2	0.34	0.136	0.024	2.024	-1.986
3	0.50	0.200	0.035	2.035	-1.922
4	0.68	0.272	0.048	2.048	-1.850
5	0.83	0.332	0.058	2.058	-1.790
6	1.00	0.400	0.070	2.070	-1.722
7	1.18	0.472	0.082	2.082	-1.650
8	1.34	0.536	0.094	2.094	-1.586
9	1.51	0.604	0.105	2.105	-1.518
10	1.71	0.684	0.119	2.119	-1.438
11	1.90	0.760	0.133	2.133	-1.362
12	2.09	0.836	0.146	2.146	-1.286
13	2.30	0.920	0.161	2.161	-1.202
14	2.52	1.008	0.176	2.176	-1.114
15	2.78	1.112	0.194	2.194	-1.010
16	3.04	1.216	0.212	2.212	-0.906
17	3.31	1.324	0.231	2.231	-0.798
18	3.64	1.456	0.254	2.254	-0.666
19	3.98	1.592	0.278	2.278	-0.530
20	4.34	1.736	0.313	2.313	-0.386
21	4.74	1.896	0.331	2.331	-0.226
22	5.20	2.080	0.363	2.363	-0.042
23	5.70	2.280	0.398	2.398	+0.158
24	6.32	2.528	0.441	2.441	+0.406
25	7.15	2.860	0.499	2.499	+0.738
26	8.06	3.224	0.562	2.562	+1.102
27	9.19	3.676	0.641	2.641	+1.554
28	10.61	4.244	0.740	2.740	+2.122

Target size - 100 yards
Target velocity - 20 yards per second
Missile velocity - 300 yards per second
Launching to cross-over range - 9000 yards
Collision range - 600 yards

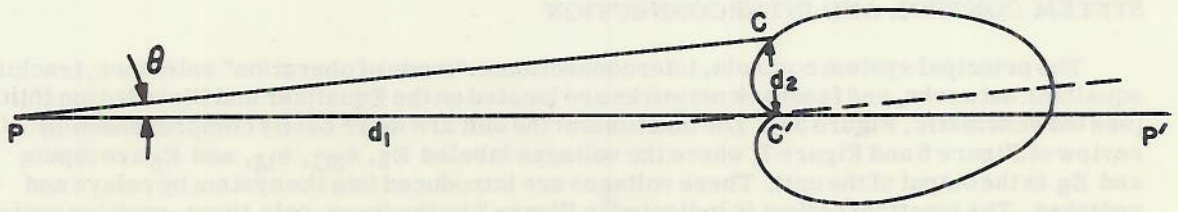

Figure 27 - Geometry of projector cam design

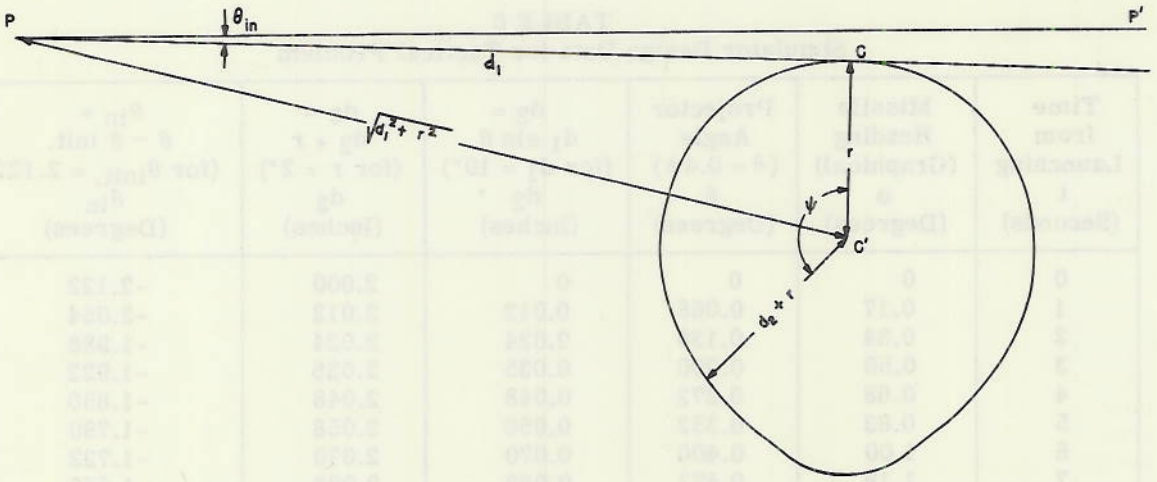

Figure 28 - Mechanization details of cam design

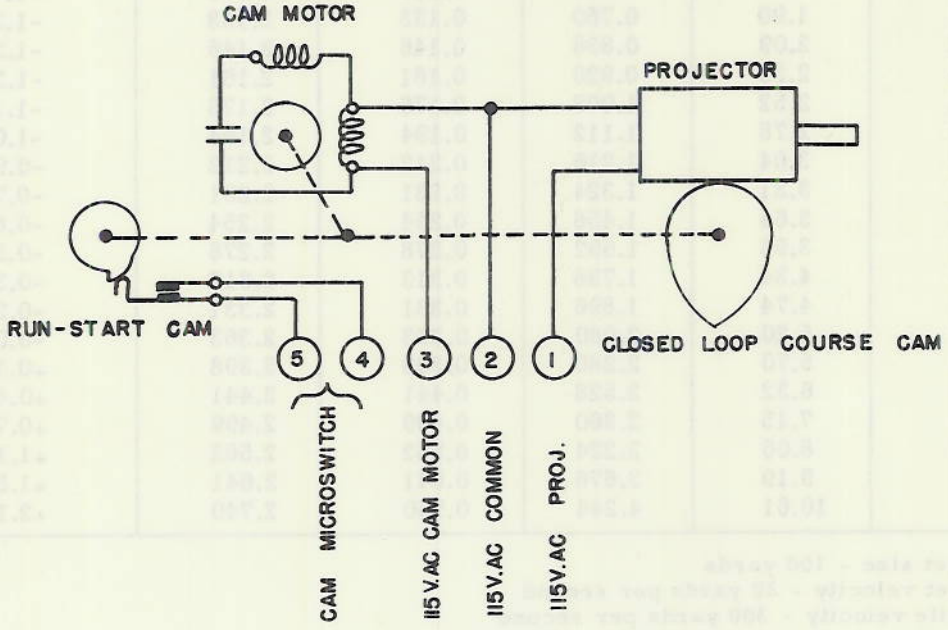

Figure 29 - Tactical course generator schematic

SYSTEM CONTROL AND INTERCONNECTION

The principal system controls, interconnections, "mode of operation" selectors, tracking equalizer networks, and feedback networks are located on the Equalizer and Distribution Unit (see the schematic, Figure 30). The functions of the unit are more easily comprehended by review of Figure 6 and Figure 7, where the voltages labeled E_2, e_{SG}, e_M, and E_6 are inputs and E_8 is the output of the unit. These voltages are introduced into the system by relays and switches. The functional effect is indicated in Figure 7 by the three-pole three-position switch. The three possible positions are labeled C (closed loop), O (open loop), and B (balance).

In the schematic, Figure 30, the switch SW 4 is a double-pole normally open push button and SW 3 is a double-pole toggle switch. These switches are used to initiate all system operational changes. The chart, Figure 31, shows the manner in which these operations occur.

SIMULATOR SERVO SYSTEM PERFORMANCE

As discussed in the earlier paragraphs on the selection of the servo system frequency response characteristics, the open-loop frequency response design objective is a single integrator or minus-one slope having a gain crossover frequency (open-loop gain of unity) at $\omega = 2$ radians per second. For low frequencies, a servo motor exhibits such a frequency response,[5] but several factors enter to prevent an increase of gain which would make the gain crossover frequency as high as desired. Variations of the load friction (gear static friction effects) and a tendency for high-frequency parasitic oscillation require a low gain setting. However, if a local feedback loop is employed, it becomes possible to raise the gain. By raising the gain, more feedback may be used, which has the effect of again lowering the gain. A proper choice of the frequency response characteristics of the local feedback path permits lowering the gain at frequencies for which the sytem tends to go into self oscillation without changing the zero-frequency gain. In this way, it is possible to achieve a high value of primary stiffness and to reduce load friction variation effects to negligible significance. The characteristics of the feedback path thus establish the performance essentially independent of any variations in the forward-loop gain.

In Figure 32, a low-frequency minus-one slope is shown crossing unity gain at $\omega_5 = 5.99$. The servo amplifier unity gain is less by the ratio $\omega_5/\omega_4 = 1.40$, shown in Figure 7 as the essentially equal value $K_{11} = 1.37$. The initial minus-one slope crossover frequency of $\omega_4 = 4.28$ is with respect to the servo amplifier only. When the local feedback loop is closed through the tachometer generator feedback network combination,[6] the asymptotic slopes (shown in Figure 33) are added, with the result that the plus-one slope starting at $\omega_2 = 2.17$ cancels the minus-one slope. At $\omega_3 = 45.5$, the minus-one slope is resumed. The over-all servo amplifier and motor transfer gain becomes (as given in Figure 7) the reciprocal of the feedback path transfer characteristic or

$$K_9\, G_9(p) = \frac{1}{\left[K_7\, G_7(p)\right]\left[K_8\, G_8(p)\right]}\,,$$

$$= 4.28\left(\frac{\omega_2 + p}{\omega_2}\right)\left(\frac{\omega_3}{\omega_3 + p}\right). \qquad (53)$$

[5] For a discussion of servo motor frequency response characteristics, see White, C. F., "Some Servo System Sinusoidal Studies," NRL Report No. R-3303, June 22, 1948.

[6] For the method of network analysis employed, see White, C. F., "Simplified Analysis of R-C and R-L Networks," NRL Report R-2668, October 15, 1945.

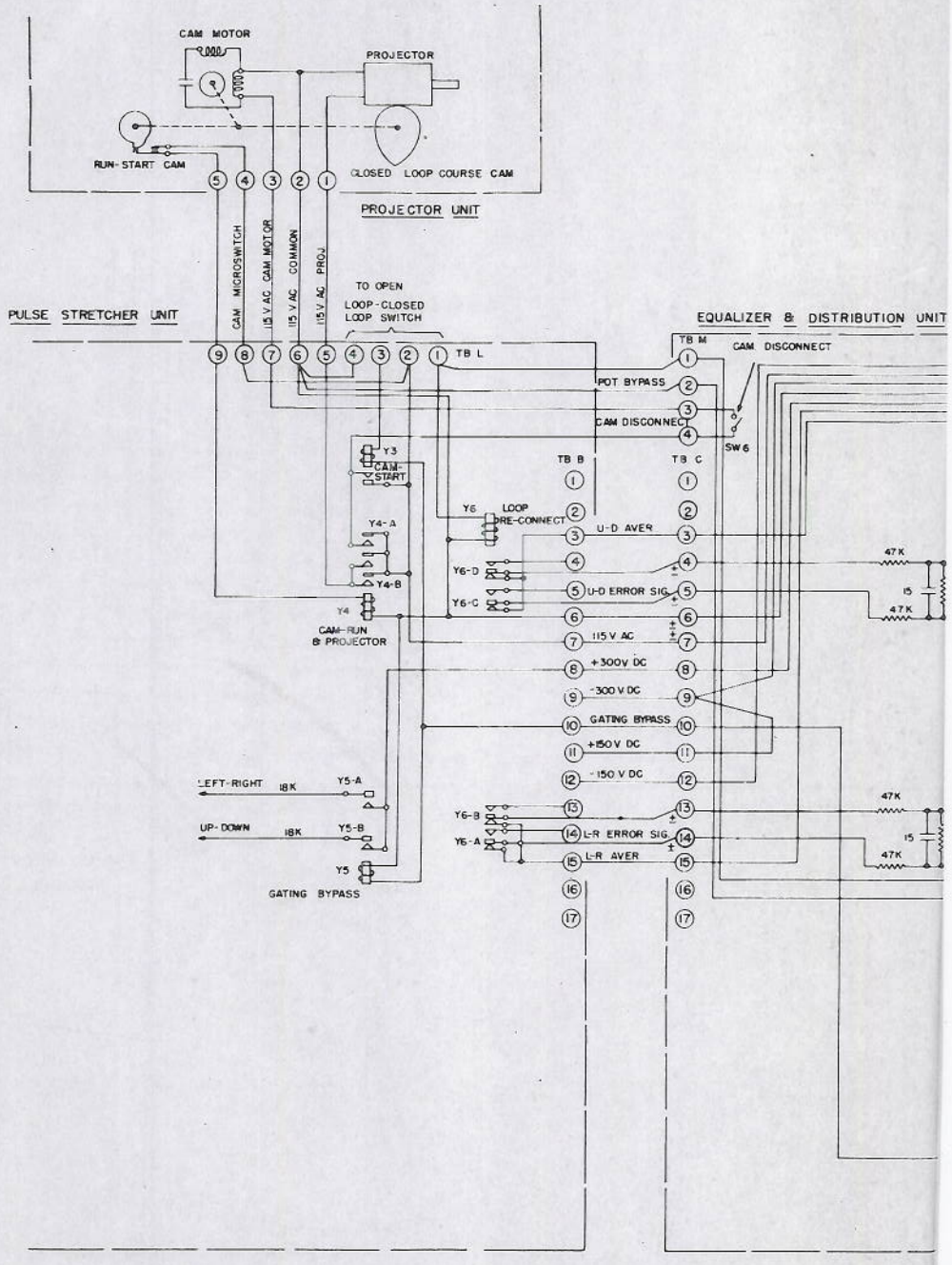

part (a) of

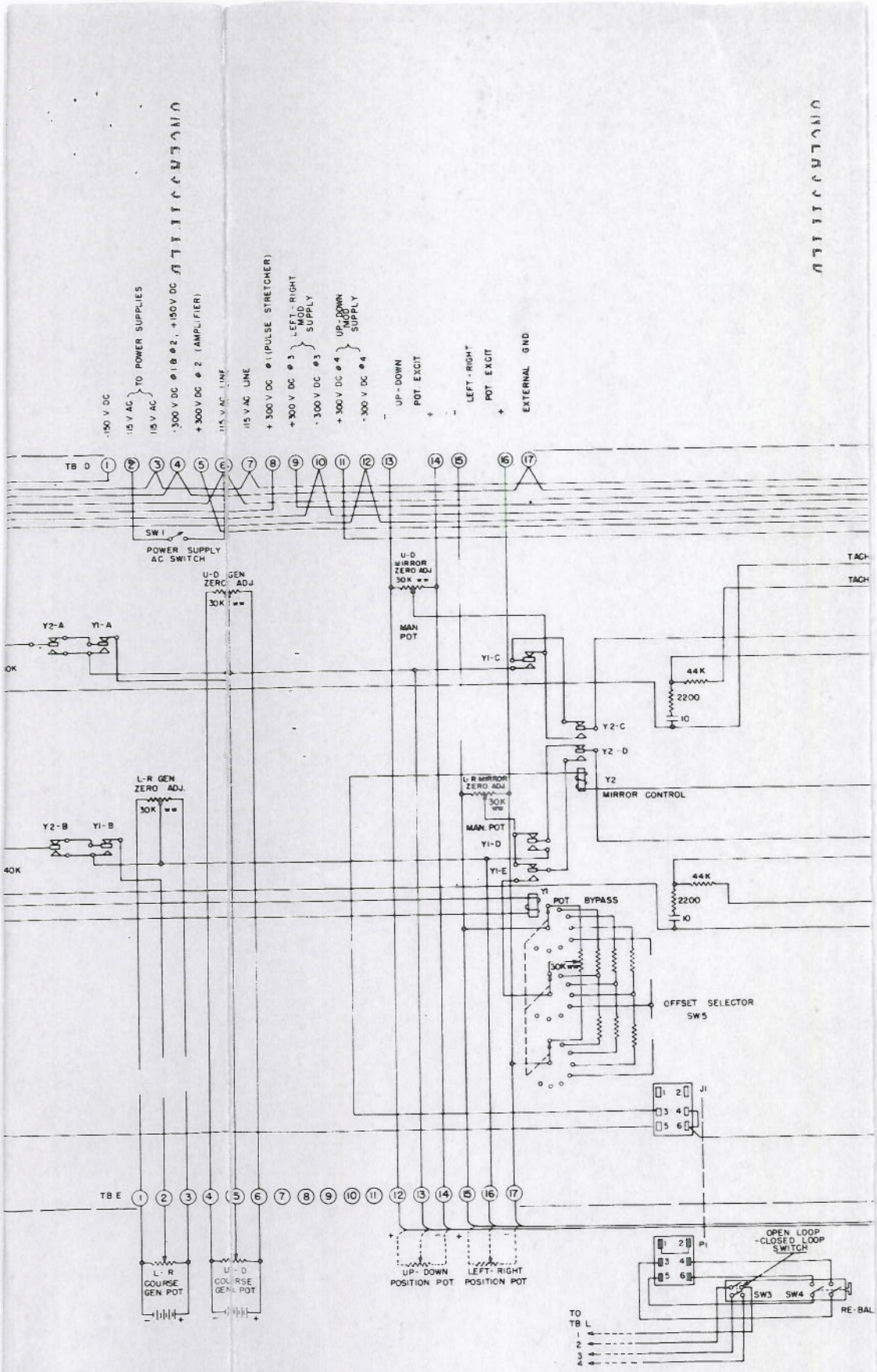

Figure 30 - System control and interconnection schematic

page 39

part (b) of page 39

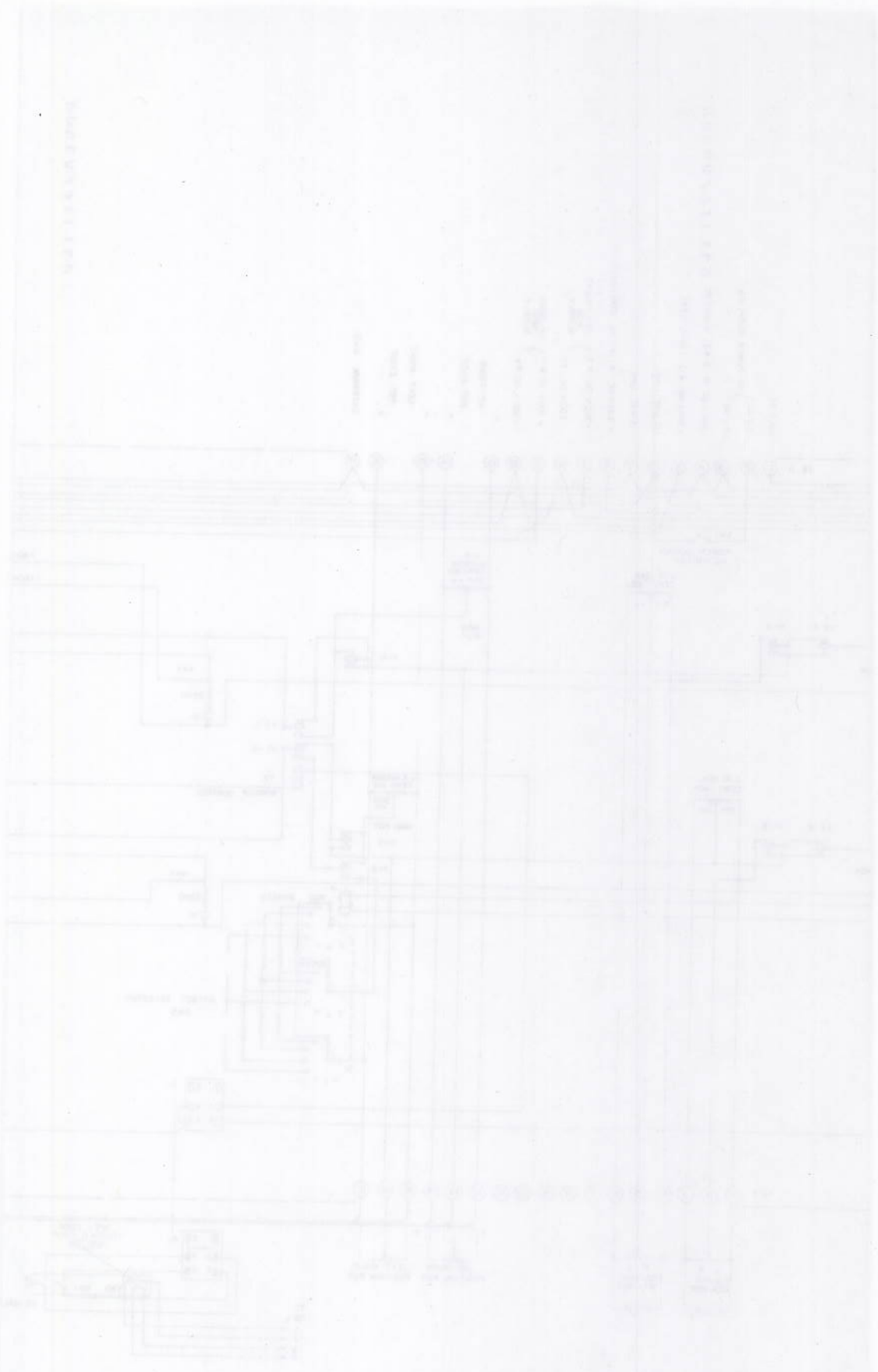

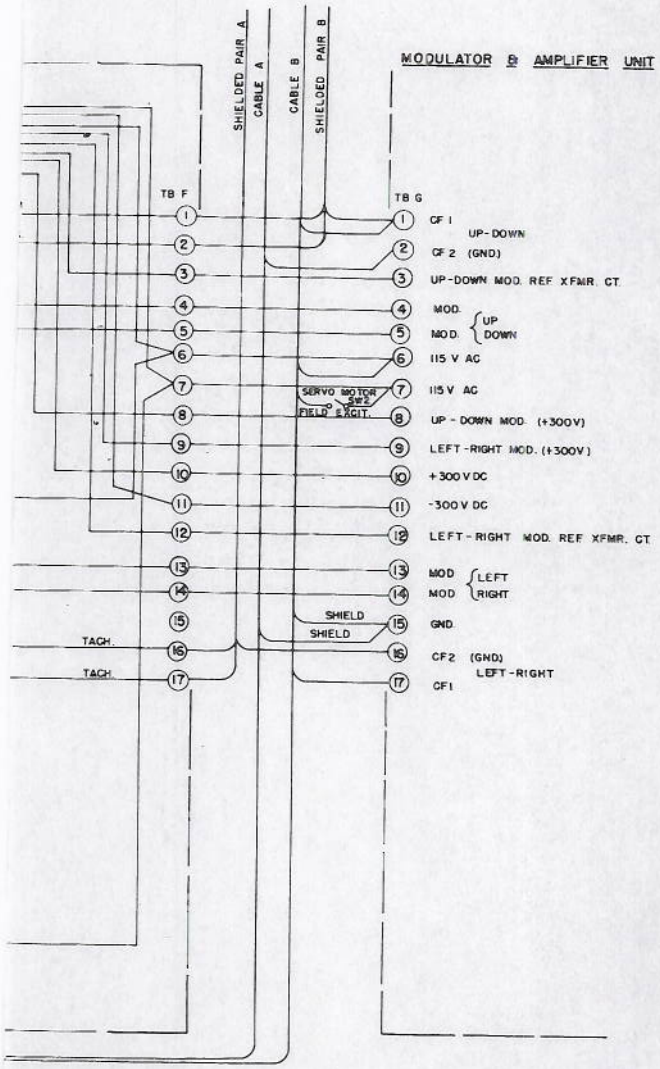

ANCE PUSH BUTTON

part (c) of page 39

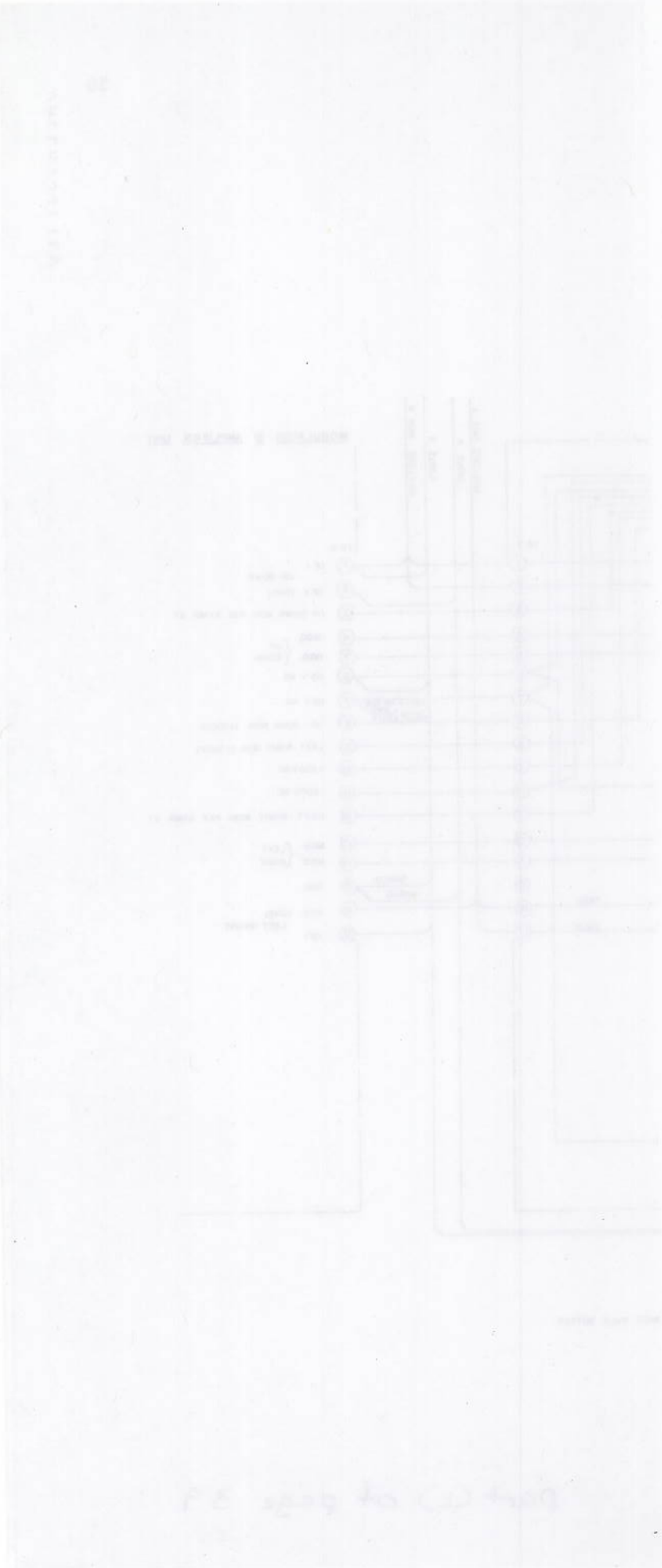

PUSH BUTTON SWITCH / TOGGLE SWITCH	UP (SWITCH CIRCUIT OPEN)		DOWN (SWITCH CIRCUIT CLOSED)	
UP (SWITCH CIRCUIT OPEN)	SIG. GEN. & REF. POTS.	MIRROR & MAN. POTS.	SIG. GEN. & REF. POTS.	MIRROR & MAN. POTS.
OPEN LOOP	IN	IN	OUT	IN
DOWN (SWITCH CIRCUIT CLOSED) CLOSED LOOP	OUT	OUT	OUT	IN (ELEV. PANEL, TRAIN: BRACKET)

Figure 31 - Mode of operation selection chart

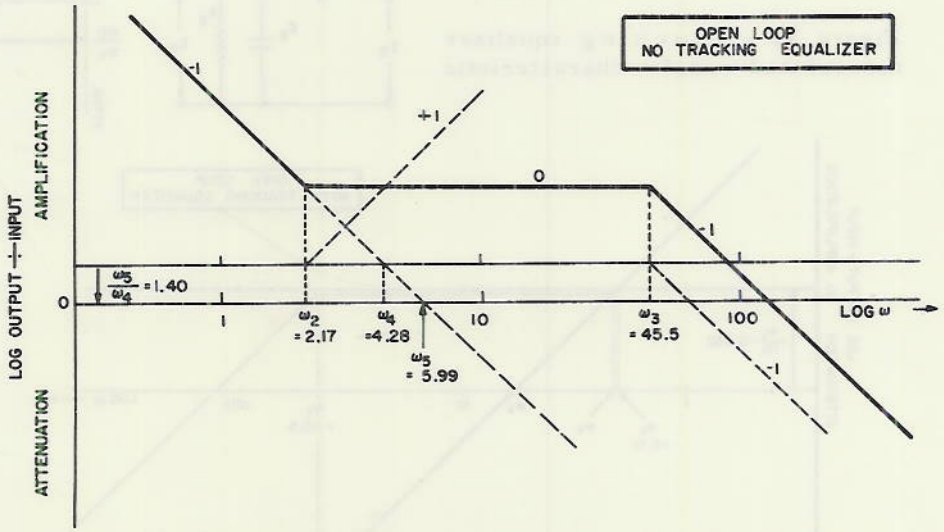

Figure 32 - Asymptotic frequency response characteristic without tracking equalizer

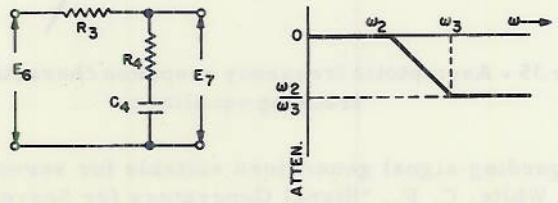

Figure 33 - Feedback network and transfer characteristic

The over-all asymptotic slope for E4 to θ_M is shown as the heavy line in Figure 32. This characteristic must be modified to a single minus-one slope passing through unity gain at $\omega = 2$ if the design objective is satisfied. The introduction of the tracking equalizer network, shown in Figure 34 together with proper loop-gain adjustment, accomplishes the desired result as shown in Figure 35. The zero slope between $\omega_2 = 2.17$ and $\omega_3 = 45.5$ is changed to a minus-one slope. The minus-one slope above $\omega_3 = 45.5$ becomes a minus-two slope. However, the ratio of

$$\frac{\omega_3}{\omega_c} = \frac{45.5}{2} = 22.7 \tag{54}$$

corresponds to approximately 27.5 decibels below unity gain before the minus-one asymptotic slope increases to the minus-two asymptotic slope. Figure 36 shows both the resulting open-loop asymptotic characteristic and the closed-loop amplitude characteristic for the simulator servo system over-all response. The results of measurements verifying the system performance are shown in Figure 37.[7] The excellent agreement between design objective and system performance is evident.

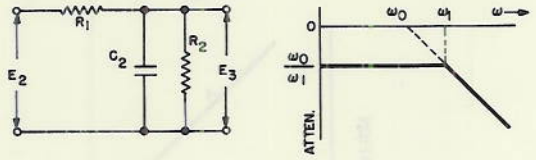

Figure 34 - Tracking equalizer network and transfer characteristic

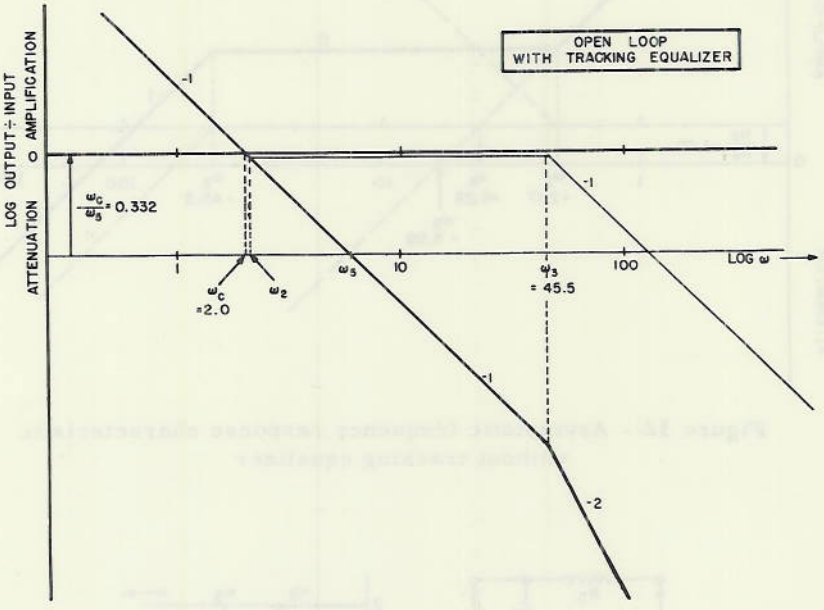

Figure 35 - Asymptotic frequency response characteristic with tracking equalizer

[7] For information regarding signal generators suitable for servo system performance measurements, see White, C. F., "Signal Generators for Servo System Measurements," Proceedings of the National Electronics Conference, 4:59-71, 1948

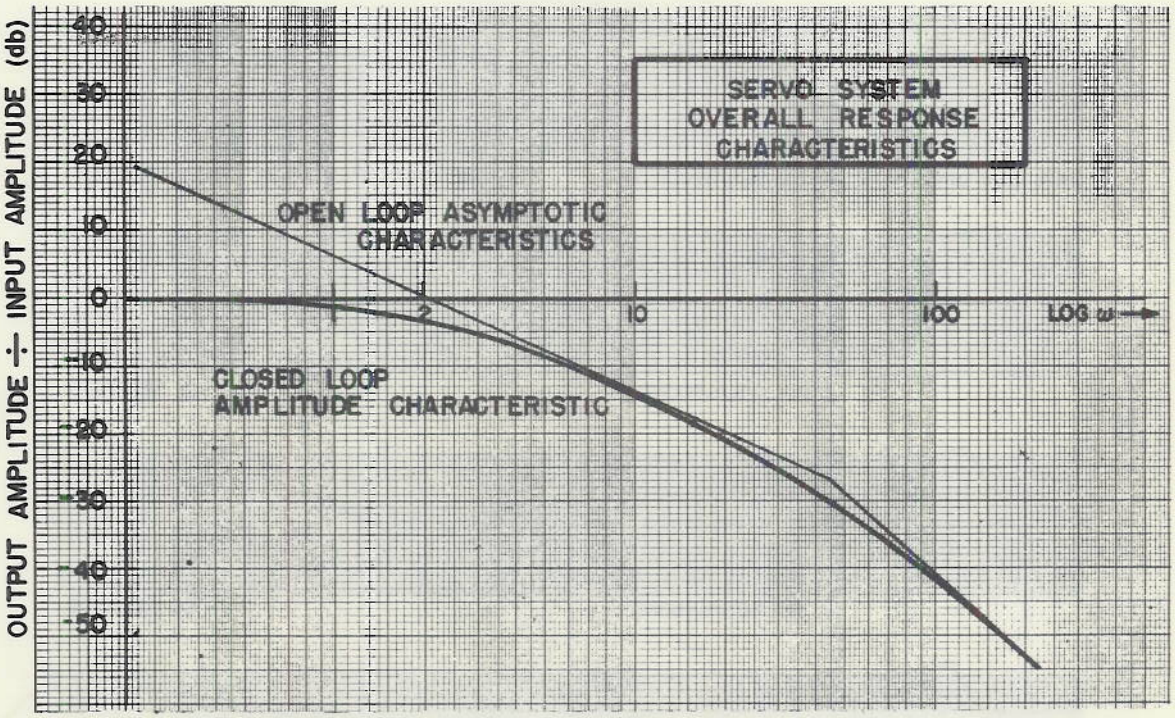

Figure 36 - Simulator servo system over-all gain characteristic

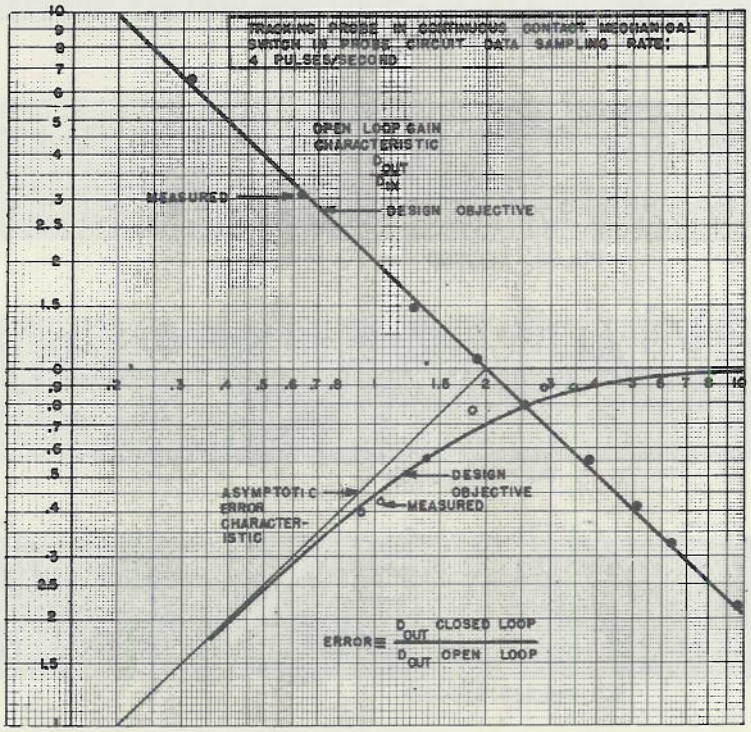

Figure 37 - Performance evaluation
of simulator servo system

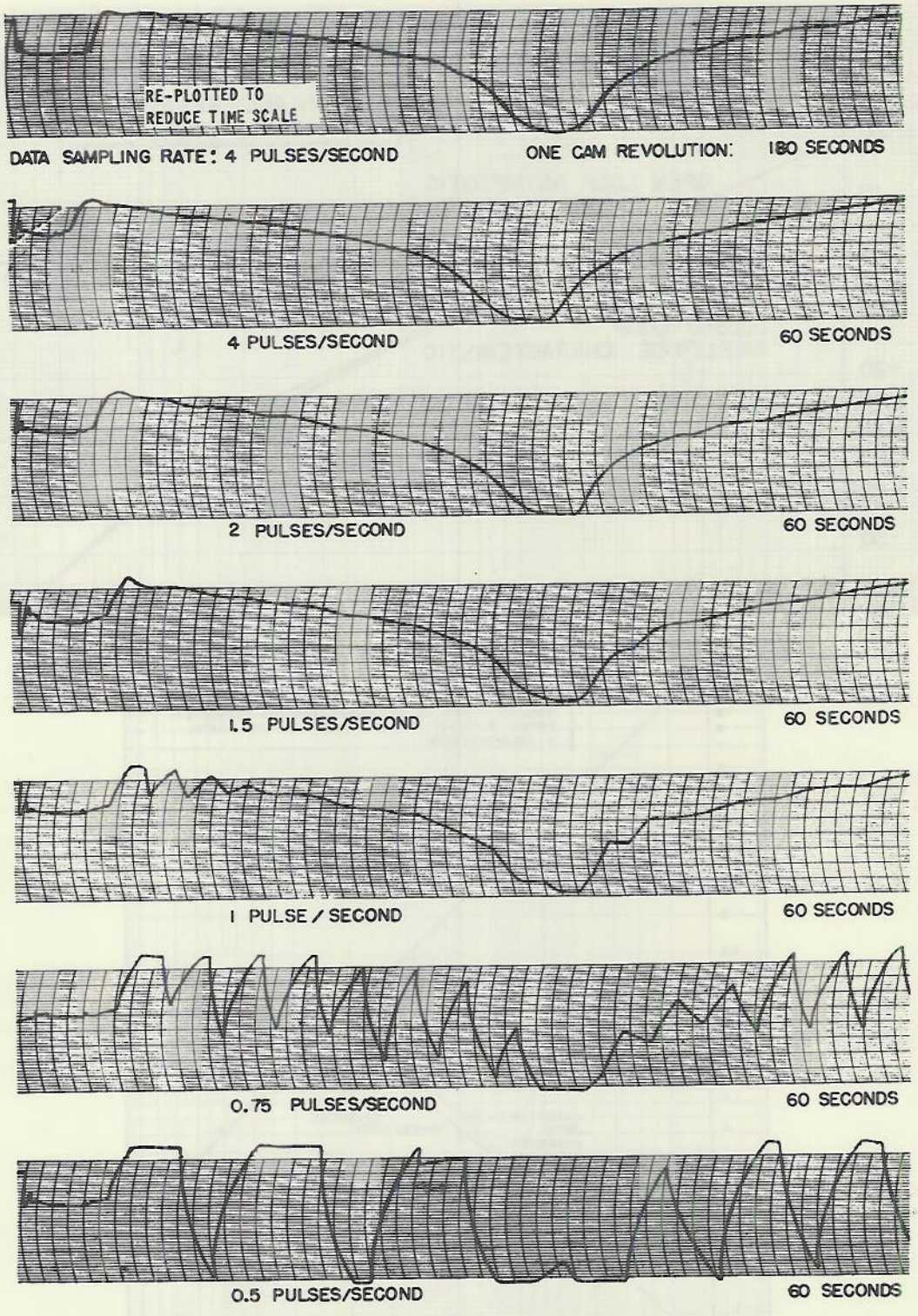

Figure 38 - Data sampling rate effects on tactical course tracking with simulator servo system bandpass of ω_c 2 radians per second

Throughout the development of the NRL ORCON Tactical Missile Simulator, the design theory utilized assumes linear performance of all components. Preliminary tests indicated that the pigeon is an approximately linear operator for target velocities below a certain value (5 inches per second) and that input motion having frequencies up to a certain value (7 radians per second) are followed with reasonable fidelity. The characteristics of the task to be performed in the simulator tests are well within the above performance limits. As the incoming information is not continuous but is in the nature of data sampling at low rates, measurements of system tracking were made for several rates.[8] The theoretical limit of modulation frequency equal to one-half carrier frequency places the lower value for transmission of any useful information as follows:

$$\text{Lower limit}_{\text{pulses/sec}} = \frac{2 \text{ pulses}}{\text{cycle}} \cdot \frac{\omega_{\text{BANDPASS}}}{2\pi} \frac{\text{cycles}}{\text{sec}},$$

$$= \frac{\omega_{\text{BANDPASS}}}{\pi} \frac{\text{pulses}}{\text{sec}} . \qquad (55)$$

For a bandpass of $\omega = 2$ radians per second, the lower limit of $2/\pi = 0.64$ pulses per second is indicated. At such a low number of pulses per second an excessive distortion occurs and the amount of the input information transmitted approaches zero. The experimental results presented in Figure 38 shows these effects strickingly. For reasonable fidelity, a rate of 1.5 to 2 pulses per second should be maintained for the 2-radian-per-second system bandwidth.

ACKNOWLEDGMENTS

Consultations with Mr. Peter Waterman, Equipment Research Branch Head, the able assistance of Mr. John M. Carl and Mr. John C. Ryon during the equipment development and construction, the mechanical design assistance of Mr. James W. Titus and the Mechanical Components Section, the cooperative efforts of Mr. Bruce H. Stafford, Operational Research Branch, and Mr. Henry P. Birmingham and Mr. Clarence L. Tipton of the Psychology Branch, and the drafting assistance of Miss Betty F. Weaver, Technical Information Division, are gratefully acknowledged.

* * *

[8] For a theoretical treatment related to the subject, see Stafford, B. H., "Frequency Analysis of Some Closed-Cycle Sampled-Data Control Systems," NRL Report No. 3910, January 1952